NASA/TM-97-206276

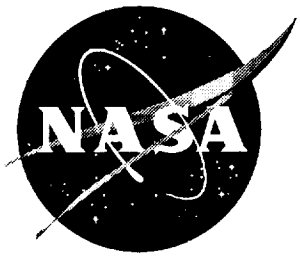

Analysis of Wind Tunnel Longitudinal Static and Oscillatory Data of the F-16XL Aircraft

Vladislav Klein, Patrick C. Murphy, Timothy J. Curry, and Jay M. Brandon

December 1997

The NASA STI Program Office ... in Profile

Since its founding, NASA has been dedicated to the advancement of aeronautics and space science. The NASA Scientific and Technical Information (STI) Program Office plays a key part in helping NASA maintain this important role.

The NASA STI Program Office is operated by Langley Research Center, the lead center for NASA's scientific and technical information. The NASA STI Program Office provides access to the NASA STI Database, the largest collection of aeronautical and space science STI in the world. The Program Office is also NASA's institutional mechanism for disseminating the results of its research and development activities. These results are published by NASA in the NASA STI Report Series, which includes the following report types:

- TECHNICAL PUBLICATION. Reports of completed research or a major significant phase of research that present the results of NASA programs and include extensive data or theoretical analysis. Includes compilations of significant scientific and technical data and information deemed to be of continuing reference value. NASA counter-part of peer reviewed formal professional papers, but having less stringent limitations on manuscript length and extent of graphic presentations.

- TECHNICAL MEMORANDUM. Scientific and technical findings that are preliminary or of specialized interest, e.g., quick release reports, working papers, and bibliographies that contain minimal annotation. Does not contain extensive analysis.

- CONTRACTOR REPORT. Scientific and technical findings by NASA-sponsored contractors and grantees.

- CONFERENCE PUBLICATION. Collected papers from scientific and technical conferences, symposia, seminars, or other meetings sponsored or co-sponsored by NASA.

- SPECIAL PUBLICATION. Scientific, technical, or historical information from NASA programs, projects, and missions, often concerned with subjects having substantial public interest.

- TECHNICAL TRANSLATION. English-language translations of foreign scientific and technical material pertinent to NASA's mission.

Specialized services that help round out the STI Program Office's diverse offerings include creating custom thesauri, building customized databases, organizing and publishing research results ... even providing videos.

For more information about the NASA STI Program Office, see the following:

- Access the NASA STI Program Home Page at ***http://www.sti.nasa.gov***

- E-mail your question via the Internet to help@sti.nasa.gov

- Fax your question to the NASA Access Help Desk at (301) 621-0134

- Phone the NASA Access Help Desk at (301) 621-0390

- Write to:
  NASA Access Help Desk
  NASA Center for AeroSpace Information
  800 Elkridge Landing Road
  Linthicum Heights, MD 21090-2934

NASA/TM-97-206276

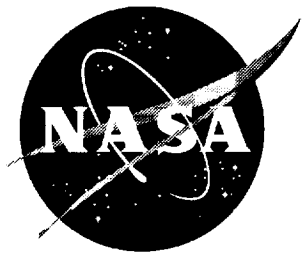

Analysis of Wind Tunnel Longitudinal Static and Oscillatory Data of the F-16XL Aircraft

Vladislav Klein
George Washington University, Hampton, Virginia

Patrick C. Murphy
NASA Langley Research Center, Hampton, Virginia

Timothy J. Curry
George Washington University, Hampton, Virginia

and

Jay M. Brandon
NASA Langley Research Center, Hampton, Virginia

National Aeronautics and
Space Administration

Langley Research Center
Hampton, Virginia 23681-2199

December 1997

Available from the following:

NASA Center for AeroSpace Information (CASI)
800 Elkridge Landing Road
Linthicum Heights, MD 21090-2934
(301) 621-0390

National Technical Information Service (NTIS)
5285 Port Royal Road
Springfield, VA 22161-2171
(703) 487-4650

SUMMARY

A wind tunnel experiment on the 10-percent-scale model of the F-16XL aircraft included longitudinal static tests, and oscillatory and ramp tests in pitch. Static tests investigated the effect of angle of attack, slideslip angle and control surface deflection on aerodynamic coefficients. For dynamic testing and analysis, the report presents data from small-amplitude oscillatory tests at nominal values of angle of attack between 20° and 60°, five frequencies from 0.6 to 2.9 Hz and one amplitude of 5°. A simple harmonic analysis provided Fourier coefficients associated with the in-phase and out-of-phase components of the aerodynamic coefficients. A strong dependence of wind tunnel oscillatory data on frequency led to the development of models with unsteady aerodynamic terms in the form of indicial functions. Two models expressing the variation of the in-phase and out-of-phase components with angle of attack and frequency were proposed and their parameters estimated from measured data. Both models with the estimated parameters were in good agreement and represented unsteady effects observed in the aerodynamic forces quite well. The estimated parameters were close to the results from the static test and both models demonstrated good prediction capability.

SYMBOLS

A	amplitude ratio
a,b_1,c	parameters in indicial function
a,b	Fourier coefficients (Appendix A)
b	wing span, m
C_L,C_N,C_m	lift, normal force, pitching-moment coefficients
$C_{L_\alpha}(t),C_{L_q}(t)$	indicial functions
$\bar{c}$	wing mean aerodynamic chord, m
f	frequency, Hz
J	cost function
k	reduced frequency, $k = \omega\ell / V$
ℓ	characteristic length, $\ell = \bar{c} / 2$
m	number of frequencies
n	number of angles of attack
n_c	number of cycles
q	pitching velocity, rad/sec
s	standard error
S	wing area, m^2
T	period, sec
T_1	time constant, $T_1 = \tau_1\ell / V$, sec
t	time, sec
u	input (Appendix A)
u,v	aerodynamic derivatives in model for in-phase and out-of-phase component of oscillatory data, respectively

$\bar{u},\bar{v}$	in-phase and out-of-phase components of oscillatory data, respectively
V	airspeed, m/sec
y	output (Appendix A)
z_u, z_v	terms in model equation (10) and (11), respectively
α	angle of attack, rad or deg
β	sideslip angle, rad or deg
Δ	increment
δ_e	elevon/flaperon deflection, rad or deg
θ	parameter in Model II
τ	time delay, sec
τ_1	nondimensional time constant, $\tau_1 = V / \ell b_1$
ϕ	phase angle, rad or deg
ω	angular frequency, rad/sec

Superscript:

$\hat{}$	estimated value

Superscript over aerodynamic derivative:

$\bar{}$	oscillatory data

Subscript:

A	amplitude
0	nominal value

Aerodynamic derivatives:

$$C_{A_a}(\infty) \equiv C_{A_a} = \frac{\partial C_A}{\partial a} \quad \text{for } A = L, N, \text{ or } m$$

$$a = \frac{q\bar{c}}{2V}, \frac{\dot{q}\bar{c}^2}{4V^2}, \alpha, \frac{\dot{\alpha}\bar{c}}{2V}, \text{ or } \delta_e$$

INTRODUCTION

For better understanding of aircraft aerodynamics in large amplitude maneuvers, NASA Langley Research Center conducted a series of wind tunnel tests on a model of the F-16XL aircraft. These tests included measurement of aerodynamic forces and moments under static conditions followed by oscillatory and ramp tests in pitch. Static measurements allowed investigation of changes in aerodynamic coefficients due to angle of attack, sideslip and control surface deflection. Dynamic testing quantified changes in aerodynamic coefficients with frequency and amplitude.

The purpose of this report is to

(a) document static and small-amplitude oscillatory data for qualitative assessment;

(b) determine a mathematical model with unsteady aerodynamic terms for oscillatory data at different angles of attack and frequencies.

The parameters in a model for small-amplitude oscillatory data were estimated by a nonlinear estimation technique of reference 1. Then, a new procedure using splines for model formulation and linear regression was applied.

The report begins with a description of the experiment. The results from static and oscillatory test are then described followed by model structure determination and parameter estimation from oscillatory data at various angles of attack and frequencies. The report is completed by concluding remarks.

MODEL AND TESTS

A three-view sketch of the 0.10-scale F-16XL model is shown in figure 1 together with some basic model dimensions. Static and dynamic tests were conducted in the NASA Langley 12-Foot Low-Speed Wind Tunnel. For both tests, the model was mounted on a dynamic test rig through a six-component strain-gauge balance. The dynamic test rig is a computer controlled,

hydraulically-actuated system which was sting-mounted on a C-strut support system. The mounting arrangement rotated the model about the reference center of gravity location of $0.558\,\bar{c}$, over an angle of attack range of $-5°$ to $80°$. The maximum capability of the dynamic test rig was 260 deg/sec pitch rate and 2290 deg/sec^2 pitch acceleration. Further description of the dynamic test rig may be found in reference 2. The tests were conducted at a dynamic pressure of 192 Pa (4 psf) resulting in a Reynolds number of 10^6 based on the mean aerodynamic chord.

All data were obtained with the leading-edge flaps at $0°$ deflection. Static data were obtained for angles of attack from $-5°$ to $80°$ at zero sideslip and zero deflection of trailing-edges surfaces (flaperons and elevons). Additional data were obtained for four values of sideslip, ($\beta = -5°$, $-10°$, $-20°$, and $-30°$), and for two values of symmetric trailing-edge control surface deflections ($\delta_e = -20°$ and $20°$). Oscillatory data were obtained at initial angles of attack (α_0) between $20°$ and $60°$ at five frequencies (0.6, 1.0, 1.41, 1.75, and 2.94 Hz) and an amplitude of $\pm 5°$. The effects of sideslip and control surface deflections were measured only at an initial angle of attack of $35°$ and two frequencies (0.6 and 1.41 Hz) at the same sideslip values and control deflections as in the static test.

Data recorded during the test runs included a linear variable differential transformer reading from the dynamic test rig to determine the pitch angle, six-component force and moment data from a strain-gauge balance, and wind tunnel dynamic pressure. Data were sampled at 100 Hz with an in-line 100 Hz low pass filter. All data channels were subsequently filtered using a 6 Hz low pass filter.

STATIC DATA

Among the measured and computed data only three aerodynamic coefficients, C_L,C_N, and C_m, are included. These coefficients are plotted against the angle of attack in figure 2. The variation of C_L with α is almost linear for $\alpha < 25°$, the maximum lift occurs at $\alpha \approx 34°$. The normal force is also changing linearly with α till $\alpha \approx 25°$, and reaches maximum value at

$\alpha \approx 38°$. The model exhibits static instability for $\alpha < 30°$. This pitch-up tendency is inherent to highly swept wings at low speeds as documented in many publications, e.g., reference 3.

Figure 3 shows the effect of sideslip on longitudinal characteristics. For $\beta < 5°$ there are almost no changes in these characteristics. Larger sideslips, however, cause a decrease in values of all coefficients, mostly in the region of α between 20° to 40°. Pitching moment decreases due to sideslip at all angles of attack $\geq 20°$. Large sideslip angles eliminate the pitch-up tendency in small segments of the angle of attack in the pre-stall region. The effect of symmetric elevon and flaperon deflection is presented in figure 4. In the post-stall region the control effectiveness is larger for negative (trailing edge up) deflection than for positive. The stability and control derivatives evaluated from the data in figure 2 and 4 with zero sideslip angle are plotted in figure 5 and 6. The control derivatives were computed for both positive and negative control deflections. From these plots a rapid decrease in control effectiveness with increased α in the post-stall region is apparent. All the measured and computed data in figures 2 to 6 are summarized in tables I to IV.

OSCILLATORY DATA

As indicated earlier, the basic set of oscillatory data was obtained at five frequencies, nine mean values of the angle of attack, α_0, and one amplitude, $\alpha_A = 5°$. The following table show the values of frequencies and the corresponding reduced frequencies selected for the test.

ω, rad/sec	f, Hz	$k = \frac{\ell}{V}\omega$
3.77	.60	.081
6.28	1.00	.134
8.86	1.41	.190
11.00	1.75	.237
18.47	2.94	.397

The mean values of α were 20.8, 25.9, 30.8, 35.8, 40.8, 45.8, 50.8 55.9 and 61.1 with the maximum deviation from these values during the repeated settings less than 0.1°.

The examples of the oscillatory data at one frequency and two mean angles of attack are given in figure 7 and 8. For $\alpha_0 = 30.8°$, the plot of $C_L(t)$ indicates a small change from a sine wave, whereas the plot of $C_m(t)$ shows the existence of at least one additional harmonic. For $\alpha_0 = 50.8°$ the departure of $C_L(t)$ from a sine wave is more pronounced and $C_m(t)$ does not resemble a simple harmonic motion at all. Further examination of the remaining time histories revealed severe distortion of measured pitching-moment coefficient at $\alpha \geq 40°$ at all frequencies, and the response can be characterized as a chaotic. The reason for this behavior has not been found yet.

For the following analysis of the oscillatory data it is assumed that the aerodynamic coefficients are linear functions of the angle of attack, pitching velocity and their rates. Then, for example, the increment in the lift coefficient with respect to its mean value can be formulated as

$$\Delta C_L = C_{L_\alpha} \Delta\alpha + \frac{\ell}{V} C_{L_{\dot\alpha}} \dot\alpha + \frac{\ell}{V} C_{L_q} q + \left(\frac{\ell}{V}\right)^2 C_{L_{\dot q}} \dot q \tag{1}$$

where for the harmonic motion

$$\begin{aligned} \Delta\alpha &= \alpha_A \sin\omega t \\ \dot\alpha &= q = \omega\alpha_A \cos\omega t \\ \ddot\alpha &= \dot q = -\omega^2 \alpha_A \sin\omega t \end{aligned} \tag{2}$$

Substitution of (2) into (1) yields

$$\begin{aligned} \Delta C_L &= \alpha_A \left(C_{L_\alpha} - k^2 C_{L_{\dot q}}\right) \sin\omega t + \alpha_A k \left(C_{L_{\dot\alpha}} + C_{L_q}\right) \cos\omega t \\ &= \alpha_A \left(\overline{C}_{L_\alpha} \sin\omega t + k\overline{C}_{L_q} \cos\omega t\right) \end{aligned} \tag{3}$$

where

$$\alpha_A \overline{C}_{L_\alpha} = \alpha_A \left(C_{L_\alpha} - k^2 C_{L_{\dot{q}}} \right) \tag{4}$$

$$\alpha_A k \overline{C}_{L_q} = \alpha_A k \left(C_{L_{\dot{\alpha}}} + C_{L_q} \right) \tag{5}$$

represent the Fourier coefficients. The in-phase and out-of-phase components of C_L($\overline{C}_{L_\alpha}$ and $\overline{C}_{L_q}$) can be obtained by integrating the time histories of ΔC_L over n_c cycles as

$$\begin{aligned} \overline{C}_{L_\alpha} &= \frac{2}{\alpha_A n_c T} \int_o^{n_c T} \Delta C_L(t) \sin \omega t \, dt \\ \overline{C}_{L_q} &= \frac{2}{\alpha_A k n_c T} \int_o^{n_c T} \Delta C_L(t) \cos \omega t \, dt \end{aligned} \tag{6}$$

where $T = 2\pi/\omega$. In the present analysis the integrals in equation (6) were obtained by a numerical technique of reference 4 applied to the last three cycles of the steady harmonic outputs.

The in-phase and out-of-phase components of all three coefficients are presented in tables V to VII and plotted against the angle of attack in figure 9. The figure shows the effect of frequency which is especially strong on the out-of-phase components. The variation of these components with the reduced frequency for two values of α_0 can be seen in figure 10. The plot of $\overline{C}_{m_q}$ for $\alpha_0 = 50.8°$ may indicate the problem with measured $C_m(t)$ mentioned earlier.

Figure 11 and 12 compare the measured coefficients C_L and C_m at one frequency and two values of α_0 with those computed from eq. (3) and (4). These coefficients are plotted against the angle of attack with time as a parameter. As shown in Appendix A, these plots should be ellipses if the formulated model given by eq. (1) is correct. Any deviation of measured $C_L(\alpha,t)$ and $C_m(\alpha,t)$ from this shape might be caused by aerodynamic nonlinearities and/or flow separation. Substantial differences between measured and computed pitching-moment coefficient exist as indicated by results in figure 11 and 12. When α and C_L are considered as the input and output variables of a dynamical system then their relationship is steady harmonic motion can be defined by the amplitude ratio and phase angle, see Appendix A. The frequency response of these quantities

for two values of α_0 is presented in figure 13. From these plots a strong effect of frequeny on the amplitude and phase within the range of k from 0 to 0.2 is apparent.

A comparison of steady and oscillatory data for all three coefficients is given in figure 14. The oscillatory data presented are for one frequency and five values of α_0 from 20 to 60°. For $\alpha_0 = 20°$ the reduction of ellipses $C_L(\alpha)$ and $C_N(\alpha)$ to almost a line is caused by small values of $\overline{C}_{L_q}$ and $\overline{C}_{N_q}$. Possible reasons for distorted ellipses has already been discussed. The effect of sideslip, elevon/flaperon deflection and tail-off configuration on the components of all three coefficients are summarized in figure 15 and 16.

PARAMETERS ESTIMATED FROM OSCILLATORY DATA

A strong dependence of wind tunnel oscillatory data on frequency lead to the development of models with unsteady aerodynamic terms, see e.g. reference 5 and 6. As an example, the model for the lift increment was formulated in reference 4 as

$$\Delta C_L = \int_o^t C_{L_\alpha}(t-\tau)\frac{d}{d\tau}\alpha d\tau + \frac{\ell}{V}\int_o^t C_{L_\alpha}(t-\tau)\frac{d}{d\tau}q(\tau)d\tau \tag{7}$$

where $C_{L_\alpha}(t)$ and $C_{L_q}(t)$ are the indicial functions.

For obtaining the model with limited number of parameters, it was assumed that the effect of $\dot{q}(t)$ on the lift could be neglected and the indicial function $C_{L_\alpha}(t)$ can be expressed as

$$C_{L_\alpha}(t) = a\left(1 - e^{-b_1 t}\right) + c \tag{8}$$

Considering the above mentioned assumptions, equation (7) is simplified as

$$\Delta C_L = C_{L_\alpha}(\infty)\alpha(t) - a\int_o^t e^{-b_1(t-\tau)}\frac{d}{d\tau}\alpha(\tau)d\tau + \frac{\ell}{V}C_{L_q}(\infty)q(t) \tag{9}$$

where $C_{L_\alpha}(\infty)$ and $C_{L_q}(\infty)$ are the rates of change of C_L with α and q in steady flow. The steady form of equation (9) for harmonic changes in α is identical to that of equation (3), that is

$$\Delta C_L(t) = \alpha_A \overline{C}_{L_\alpha} \sin\omega t + \alpha_A k \overline{C}_{L_q} \cos\omega t \tag{3}$$

However, with the indicial function of equation (8), the expressions for $\overline{C}_{L_\alpha}$ and $\overline{C}_{L_q}$ have the form

$$\overline{C}_{L_\alpha} = C_{L_\alpha}(\infty) - a\frac{\tau_1^2 k^2}{1+\tau_1^2 k^2} \tag{10}$$

$$\overline{C}_{L_q} = C_{L_q}(\infty) - a\frac{\tau_1}{1+\tau_1^2 k^2} \tag{11}$$

where $\tau_1 = V/b_1 \ell$ is the nondimensional time constant.

From the experiment, the in-phase and out-of-phase components are usually obtained for different values of the angle of attack and reduced frequency while keeping the amplitude of the oscillations constant. Then the equations (10) and (11) can be generalized as

$$\overline{u}_{ji} = u_i - a_i z_{u_j} \tag{12}$$

$$\overline{v}_{ji} = v_i - a_i z_{v_j} \tag{13}$$

These equations define Model I where for the lift coefficient

$$u_i = C_{L_\alpha}(\alpha_i) \qquad v_i = C_{L_q}(\alpha_i)$$

$$z_{u_j} = \frac{\tau_1^2 k_j^2}{1+\tau_1^2 k_j^2} \qquad z_{v_j} = \frac{\tau_1}{1+\tau_1^2 k_j^2}$$

$$\text{for} \quad \begin{matrix} \text{i} = 1,2,\ldots,\text{n} \\ \text{j} = 1,2,\ldots,\text{m} \end{matrix}$$

In equations (12) and (13) there are, in general, $3n+1$ unknown parameters: u_i, v_i, a_i and τ_1. They can be estimated from experimental data $\overline{u}_{ji}$ *and* $\overline{v}_{ji}$ by minimizing the cost function

$$J_I = \sum_{j=1}^{m}\sum_{i=1}^{n}\left\{\left[\overline{u}_{ji} - \left(u_i - a_i z_{u_j}\right)\right]^2 + \left[\overline{v}_{ji} - \left(v_i - a_i z_{v_j}\right)\right]^2\right\} \tag{14}$$

More about the estimation procedure can be found in reference 1.

In formulating airplane equations of motion it might be more convenient to obtain expressions for u, v, and a as a function of the angle of attack rather than their discrete values. For that reason the previous model was reformulated as Model II defined by the following equations:

$$\bar{u}_{ji} = u(\alpha_i) - a(\alpha_i) z_{u_j} \tag{15}$$

$$\bar{v}_{ji} = v(\alpha_i) - a(\alpha_i) z_{v_j} \tag{16}$$

The form of expressions for $u(\alpha_i)$, $v(\alpha_i)$and $a(\alpha_i)$ can be either specified from the variation of estimated parameters in Model I or the form can be postulated in terms of polynomials and/or polynomial splines. In the second case adequate models for $u(\alpha), v(\alpha)$ and $a(\alpha)$ can be determined from measured data by a stepwise regression. The previously estimated value of parameter τ_1 can be used as an *a priori* value thus simplifying the parameter estimation procedure using Model II and the cost function

$$J_{II} = \sum_{j=1}^{m} \sum_{i=1}^{n} \left\{ \left[\bar{u}_{ji} - \left(u(\alpha_i) - a(\alpha_i) z_{uj} \right) \right]^2 + \left[\bar{v}_{ji} - \left(v(\alpha_i) - a(\alpha_i) z_{vi} \right) \right]^2 \right\} \tag{17}$$

Both estimation procedures were applied to oscillatory data at four frequencies and nine value of the angle of attack. The measured data for frequency $k = .190$ were not included in the estimation. This set of data was used to demonstrate the model prediction capabilities. The estimated parameters u_i, v_i, and a_i in Model I are plotted in figures 17 to 19. In these figures, the 2s confidence intervals for parameter estimates are also included. The minimum and maximum values of standard errors are summarized in Table VIII. The parameters $C_{L_\alpha}(\infty)$ and $C_{N_\alpha}(\infty)$ are in good agreement with those from static data displayed in figure 5. There is, however, large discrepancy between $C_{m_\alpha}(\infty)$ from oscillatory and static data caused by problems in measured

time histories $C_m(t)$, as discussed earlier. No values, theoretical or experimental, were available for derivatives C_{L_q}, C_{N_q} and C_{m_q} for comparison with results from oscillatory tests. The parameter values a_i indicate smooth variation of unsteady terms with α and the largest effect of unsteady terms on the coefficients at α around 40°. The estimated values of τ_1, and computed values of parameter b_1 and T_1 are presented in Table IX together with their standard errors. These results indicate that the time constant associated with the unsteady effects is about 0.4 sec. for the lift and normal force, and about 0.6 sec for the pitching moment.

A comparison of measured in-phase and out-of-phase components of all three coefficients with those estimated is given in figures 20 to 22. The predicted components computed from model equations (10) and (11) for $k = .190$ are presented in figure 23 to 25 together with the corresponding measured values. These figures demonstrate that Model I for C_L and C_N is a good predictor. No conclusion about predicted values of $\overline{C}_{m_\alpha}$ and $\overline{C}_{m_q}$ can be made because of chaotic behavior of measured values $\overline{C}_m(t)$ at $\alpha \geq 40°$.

Expressions for terms $u(\alpha), v(\alpha)$ and $a(\alpha)$ in Model II for the lift coefficient were selected from results in figure 26 as

$$\begin{aligned} C_{L_\alpha}(\alpha) &\equiv u(\alpha) = \theta_0 + \theta_1\alpha + \theta_2\alpha^2 + \theta_3(\alpha - 0.803)_+^2 \\ C_{L_q}(\alpha) &\equiv v(\alpha) = \theta_4 + \theta_5\alpha + \theta_6\alpha^2 \\ a(\alpha) &= \theta_7 + \theta_8\alpha + \theta_9\alpha^2 + \theta_{10}(\alpha - 0.803)_+^2 \end{aligned} \tag{18}$$

where

$$\begin{aligned} (\alpha - 0.803)_+^2 &= 0 \text{ for } \alpha \leq 0.803 \\ &= (\alpha - 0.803)^2 \quad \text{for } \alpha \geq 0.803 \end{aligned}$$

An identical model was postulated for the normal-force coefficient. There was no attempt to estimate parameters in the pitching-moment equations.

The parameters in equations (18) were obtained by a linear regression for given values of parameter τ_1. The mean values and standard errors of the estimates are summarized in table X.

The results indicate parameter uncertainty in expressions for $C_{L_q}(\alpha)$ and $C_{N_q}(\alpha)$. Low accuracy of these parameters could result from small number of data points and their small sensitivity due to small magnitudes of C_{L_q} and C_{N_q}. The estimated terms of the in-phase and out-of-phase components are plotted in figures 26 and 27, and compare with estimated parameters in Model I. The agreement between both sets of results is very good. The measured and estimated components of C_L and C_N are presented in figure 28 and 29. With the exception of $\overline{C}_{L_\alpha}$ and $\overline{C}_{N_\alpha}$ for $k = 0.397$ and 0.081, the estimated components are close to the measured values. Finally, figure 30 and 31 demonstrate prediction capabilities of Model II which are as good as those of Model I.

CONCLUDING REMARKS

A wind tunnel experiment on a 10-percent-scale model of the F-16XL aircraft was conducted at NASA Langley Research Center. This experiment concluded longitudinal static and oscillatory tests. Static tests investigated the effect of the angle of attack, sideslip angle and control surface deflection on aerodynamic coefficients from which only the lift, normal-force and pitching moment are presented in this report. The variation of lift with angle of attack was found to be almost linear for angles of attack less than 25°; the maximum lift occurred at an angle of attack of about 34°. Similar results were obtained for the normal force. The model exhibited static instability for angles of attack less than 30°. For small sideslip angles, less than 5°, there were almost no changes in the longitudinal characteristics. Large sideslips, however, caused a decrease in values of all coefficients. Changes in symmetric elevon and flaperon deflections indicated that in the post-stall region the control effectiveness was larger for negative (trailing-edge-up) deflections than for the opposite defections.

For dynamic testing and analysis, the report presents only data from small-amplitude oscillatory tests at nominal values of angle of attack between 20° and 60°, five frequencies from 0.6 to 20.9 Hz and one amplitude of 5°. A limited amount of data exhibiting the effect of sideslip angle, control surface defection and tail-off configuration is also included without any discussion.

Time histories of the lift and normal force coefficients for angle of attack greater than 30° indicated relatively large changes from a sine wave, probably caused by aerodynamic nonlinearities. The time histories of the pitching moment, however, did not resemble a simple haromonic response at all. With increasing angles of attack these time histories were getting closer to chaotic motion. Regardless of these irregularities in time histories, it was assumed that for data analysis the aerodynamic coefficients were linear functions of the angle of attack, pitching velocity and their rates. Then, a simple harmonic analysis over three cycles of oscillation provided the Fourier coefficients associated with the in-phase and out-of-phase components of the coefficients. These components were plotted against the angle of attack for a given value of reduced frequency.

A strong dependence of wind tunnel oscillatory data on frequency led to the development of models with unsteady aerodynamic terms in the form of indicial functions. These functions were postulated as simple exponentials where the unknown parameters included aerodynamic derivatives, the exponents and multiplication terms. Two models expressing the variation of the in-phase and out-of-phase components with the angle of attack and frequency were proposed. In the first model, the unknown parameters, including the exponent, were estimated from measured data by a nonlinear least squares technique at nominal values of angle of attack. In the second model, polynomial splines expressing the variation of unknown parameters with the angle of attack were formulated and their parameters estimated by linear least squares technique for a known value of the exponent. Both models with the estimated parameters were in good agreement and represented unsteady effects observed in the lift and normal force quite well. In addition, some of the estimated parameters were close to the results from the static test and both models demonstrated good prediction capabilities.

REFERENCES

1. Klein, Vladislav and Noderer, Keith D.: Modeling of Aircraft Unsteady Aerodynamic Characteristics. Part II—Parameters Estimated From Wind Tunnel Data, NASA TM 110161, 1995.
2. Brandon, J. M.: Dynamic Stall Effects and Application to High Performance Aircraft. Special Course on Aircraft Dynamics at High Angles of Attack: Experiment and Modeling. AGARD Report No. 776, April 1991, pp. 2-1 to 2-15.
3. Wedekind, G.: Influence of Configuration Components of Statically Unstable Combat Aircraft on the Aerodynamic Design for High Angles-of-Attack. AGARD-LS-121, 1982, pp. 11–1 to 11–33.
4. Morelli, Eugene A.: High Accuracy Evaluation of the Finite Fourier Transform using Sampled Data. NASA TM 110340, 1997.
5. Klein, Vladislav and Noderer, Keith D.: Modeling of Aircraft Unsteady Aerodynamic Characteristics. Part I—Postulated Models, NASA TM 109120, 1994.
6. Goman, M. and Khrabrov, A.: State-Space Representation of Aerodynamic Characteristics of an Aircraft at High Angles of Attack. Journal of Aircraft, Vol. 31, No. 5, 1994, pp. 1109–1115.

APPENDIX A

HARMONIC MOTION

Let the input to a linear, time-invariant, dynamical system be

$$u = \alpha_A \sin \omega t \tag{A1}$$

Then the steady state output of the system has the form

$$\begin{aligned} y &= a\sin \omega t + b\cos\omega t \\ &= A\sin(\omega t - \phi) \end{aligned} \tag{A2}$$

where

$$\begin{aligned} a &= A\cos\phi \\ b &= -A\sin\phi \end{aligned} \tag{A3}$$

and

$$\begin{aligned} A^2 &= a^2 + b^2 \\ \tan\phi &= -\frac{b}{a} \end{aligned} \tag{A4}$$

Replacing y by ΔC_L and u by α it follows from equations (A3), (A4) and (3) that

$$\begin{aligned} a &= \alpha_A \overline{C}_{L_\alpha} \\ b &= \alpha_A k \overline{C}_{L_q} \end{aligned} \tag{A5}$$

and the expression for amplitude ratio and phase angle takes the form

$$A = \alpha_A \sqrt{\overline{C}_{L_\alpha}^2 + k^2 \overline{C}_{L_q}^2} \tag{A6}$$

$$\phi = \tan^{-1}\left(-\frac{k\overline{C}_{L_q}}{\overline{C}_{L_\alpha}}\right) \tag{A7}$$

Returning to equations (A1) and (A2), and considering unit amplitude of the input variable

$$\begin{aligned} y &= a\sin\omega t + b\cos\omega t \\ &= a\sin\omega t + b\sqrt{1-\sin^2\omega t} \\ &= au + b\sqrt{1-u^2} \end{aligned} \tag{A8}$$

Taking square of both sides of (A8) yields

$$y^2 - 2auy + \left(a^2 + b^2\right)u^2 = b^2 \tag{A9}$$

Replacing again y by ΔC_L and u by α in equation (A9), and using, equation (A5) gives

$$\Delta C_L^2 - 2C_{L_\alpha}\Delta C_L\alpha + \left(\overline{C}_{L_\alpha}^2 + k^2\overline{C}_{L_q}^2\right)\alpha^2 = k^2\overline{C}_{L_q}^2 \tag{A10}$$

The discriminant of eq. (A10) is

$$\begin{vmatrix} 1 & -\overline{C}_{L_\alpha} \\ -\overline{C}_{L_\alpha} & \overline{C}_{L_\alpha}^2 + k^2\overline{C}_{L_q}^2 \end{vmatrix} = k^2\overline{C}_{L_q}^2 > 0$$

which means that eq. (A10) represents an ellipse. For $k\overline{C}_{L_q}^2 = 0$ the ellipse is reduced to a line as follows from (A8).

α, deg	$\beta = 0°$ $\delta_e = 0°$	$\beta = -5°$ $\delta_e = 0°$	$\beta = -10°$ $\delta_e = 0°$	$\beta = -20°$ $\delta_e = 0°$	$\beta = -30°$ $\delta_e = 0°$	$\beta = 0°$ $\delta_e = 20°$	$\beta = 0°$ $\delta_e = -20°$
-4.0000	-0.1000	-0.1052	-0.1041	-0.1102	-0.0877	0.2025	-0.4338
0.0000	0.0535	0.0500	0.0478	0.0380	0.0427	0.3555	-0.2586
5.0000	0.2590	0.2546	0.2484	0.2337	0.2249	0.5981	-0.0692
10.0000	0.4977	0.4959	0.4781	0.4425	0.4202	0.8221	0.1357
15.0000	0.7470	0.7447	0.7181	0.6625	0.6119	1.0309	0.3637
20.0000	0.9774	0.9831	0.9672	0.8482	0.8041	1.2382	0.6066
22.0000	1.0543	1.0919	1.0545	0.8800	0.8358	1.3285	0.6879
24.0000	1.1468	1.1593	1.1202	0.9199	0.8523	1.3994	0.7718
26.0000	1.2070	1.2258	1.1604	0.9724	0.8629	1.4422	0.8462
28.0000	1.2529	1.2716	1.1700	1.0138	0.8374	1.4577	0.9033
30.0000	1.2726	1.2718	1.1916	1.0029	0.8447	1.4314	0.9484
32.0000	1.2780	1.2696	1.1907	0.9668	0.8594	1.3981	0.9811
34.0000	1.2650	1.2613	1.1988	0.9926	0.8588	1.3553	1.0126
36.0000	1.2388	1.2233	1.1806	1.0152	0.8556	1.3389	1.0192
38.0000	1.2143	1.1374	1.1376	1.0244	0.8682	1.2628	1.0033
40.0000	1.1347	1.0445	1.0513	1.0237	0.8860	1.1145	0.9366
45.0000	0.9255	0.8813	0.8833	0.8518	0.8402	0.9767	0.7748
50.0000	0.8377	0.8235	0.8153	0.7826	0.7547	0.8798	0.7037
60.0000	0.7202	0.7046	0.6852	0.6658	0.6289	0.7027	0.5963
70.0000	0.5403	0.5240	0.5048	0.4967	0.4616	0.5004	0.4553
80.0000	0.2950	0.2894	0.2850	0.2742	0.2567	0.2331	0.2629

Table I. Effect of angle of attack, sideslip, and elevons and flaperons on lift coefficient.

α, deg	$\beta = 0^\cdot$ $\delta_e = 0^\cdot$	$\beta = -5^\cdot$ $\delta_e = 0^\cdot$	$\beta = -10^\cdot$ $\delta_e = 0^\cdot$	$\beta = -20^\cdot$ $\delta_e = 0^\cdot$	$\beta = -30^\cdot$ $\delta_e = 0^\cdot$	$\beta = 0^\cdot$ $\delta_e = 20^\cdot$	$\beta = 0^\cdot$ $\delta_e = -20^\cdot$
-4.0000	-0.1022	-0.1075	-0.1064	-0.1123	-0.0899	0.1980	-0.4403
0.0000	0.0535	0.0500	0.0478	0.0380	0.0427	0.3555	-0.2586
5.0000	0.2612	0.2568	0.2505	0.2358	0.2274	0.6055	-0.0639
10.0000	0.5058	0.5040	0.4858	0.4499	0.4283	0.8426	0.1469
15.0000	0.7714	0.7690	0.7414	0.6847	0.6346	1.0769	0.3875
20.0000	1.0335	1.0400	1.0232	0.8991	0.8545	1.3297	0.6553
22.0000	1.1269	1.1689	1.1291	0.9456	0.9008	1.4459	0.7512
24.0000	1.2416	1.2575	1.2155	1.0035	0.9333	1.5457	0.8534
26.0000	1.3256	1.3495	1.2794	1.0775	0.9608	1.6195	0.9491
28.0000	1.3993	1.4245	1.3135	1.1430	0.9508	1.6677	1.0306
30.0000	1.4480	1.4526	1.3638	1.1467	0.9779	1.6715	1.1021
32.0000	1.4839	1.4809	1.3915	1.1362	1.0147	1.6692	1.1637
34.0000	1.5012	1.5044	1.4320	1.1921	1.0360	1.6567	1.2267
36.0000	1.5046	1.4968	1.4447	1.2478	1.0557	1.6773	1.2634
38.0000	1.5115	1.4311	1.4298	1.2908	1.0972	1.6268	1.2749
40.0000	1.4546	1.3533	1.3597	1.3254	1.1484	1.4834	1.2268
45.0000	1.2840	1.2354	1.2374	1.1949	1.1730	1.4104	1.1051
50.0000	1.2674	1.2604	1.2460	1.2033	1.1561	1.3962	1.0979
60.0000	1.3642	1.3566	1.3196	1.2935	1.2230	1.4325	1.1702
70.0000	1.4411	1.4347	1.3916	1.3736	1.2955	1.5044	1.2660
80.0000	1.4643	1.5223	1.4958	1.4383	1.3444	1.5504	1.3743

Table II. Effect of angle of attack, sideslip, and elevons and flaperons on normal-force coefficient.

α, deg	$\beta = 0^\cdot$ $\delta_e = 0^\cdot$	$\beta = -5^\cdot$ $\delta_e = 0^\cdot$	$\beta = -10^\cdot$ $\delta_e = 0^\cdot$	$\beta = -20^\cdot$ $\delta_e = 0^\cdot$	$\beta = -30^\cdot$ $\delta_e = 0^\cdot$	$\beta = 0^\cdot$ $\delta_e = 20^\cdot$	$\beta = 0^\cdot$ $\delta_e = -20^\cdot$
-4.0000	0.0201	0.0156	0.0265	0.0163	0.0237	-0.0627	0.0937
0.0000	0.0242	0.0270	0.0318	0.0261	0.0329	-0.0558	0.0998
5.0000	0.0441	0.0458	0.0476	0.0428	0.0515	-0.0479	0.1204
10.0000	0.0733	0.0744	0.0755	0.0702	0.0764	-0.0095	0.1525
15.0000	0.1107	0.1107	0.1110	0.1040	0.1035	0.0385	0.1940
20.0000	0.1530	0.1531	0.1515	0.1458	0.1051	0.0855	0.2359
22.0000	0.1685	0.1734	0.1679	0.1605	0.1248	0.1047	0.2521
24.0000	0.1858	0.1880	0.1841	0.1574	0.1470	0.1246	0.2694
26.0000	0.2009	0.2059	0.1970	0.1726	0.1627	0.1437	0.2834
28.0000	0.2161	0.2214	0.1995	0.1938	0.1577	0.1603	0.2931
30.0000	0.2244	0.2243	0.2094	0.1985	0.1476	0.1680	0.2977
32.0000	0.2256	0.2238	0.2168	0.1771	0.1377	0.1700	0.2966
34.0000	0.2214	0.2222	0.2196	0.1738	0.1357	0.1708	0.2987
36.0000	0.2183	0.2164	0.2162	0.1822	0.1407	0.1773	0.2955
38.0000	0.2186	0.2020	0.2068	0.1863	0.1460	0.1698	0.2891
40.0000	0.1995	0.1890	0.1943	0.1926	0.1479	0.1478	0.2631
45.0000	0.1867	0.1728	0.1750	0.1701	0.1664	0.1594	0.2431
50.0000	0.1793	0.1634	0.1596	0.1462	0.1386	0.1596	0.2386
60.0000	0.1578	0.1493	0.1386	0.1371	0.1144	0.1374	0.2114
70.0000	0.1208	0.1181	0.1065	0.1074	0.0794	0.1093	0.1706
80.0000	0.0594	0.0466	0.0428	0.0560	0.0479	0.0458	0.0963

Table III. Effect of angle of attack, sideslip, and elevons and flaperons on pitching-moment coefficient.

α, deg	$C_{L\alpha}$	$C_{N\alpha}$	$C_{m\alpha}$	$C_{L\delta e}$	$C_{N\delta e}$	$C_{m\delta e}$
-4.000	2.200	2.250	-0.040	0.911	0.917	-0.223
0.000	2.230	2.290	0.131	0.882	0.882	-0.223
5.000	2.520	2.590	0.280	0.957	0.957	-0.241
10.000	2.780	2.880	0.376	0.986	0.997	-0.235
15.000	2.770	3.030	0.451	0.957	0.986	-0.223
20.000	2.390	2.850	0.466	0.905	0.968	-0.218
22.000	2.234	2.808	0.459	0.917	0.997	-0.212
24.000	1.947	2.622	0.429	0.900	0.991	-0.206
26.000	1.436	2.175	0.369	0.854	0.963	-0.201
28.000	1.021	1.803	0.295	0.796	0.911	-0.189
30.000	0.479	1.280	0.168	0.693	0.814	-0.183
32.000	-0.064	0.761	0.019	0.596	0.722	-0.183
34.000	-0.479	0.314	-0.070	0.493	0.619	-0.183
36.000	-0.989	-0.207	-0.100	0.458	0.590	-0.172
38.000	-1.500	-0.766	-0.212	0.372	0.504	-0.172
40.000	-2.010	-1.400	-0.264	0.292	0.367	-0.166
45.000	-1.590	-0.952	-0.100	0.287	0.435	-0.120
50.000	-0.830	0.165	-0.100	0.252	0.430	-0.115
60.000	-0.830	0.537	-0.160	0.183	0.378	-0.109
70.000	-1.240	0.277	-0.286	0.143	0.344	-0.086
80.000	-1.560	-0.021	-0.435	0.103	0.252	-0.074

Table IV. Effect of angle of attack on stability and control parameters.

Component	α, deg	k = .081	k = .135	k = .190	k = .237	k = .397
$\overline{C}_{L_\alpha}$	20.8	2.7173	2.7262	2.7169	2.6812	2.7182
	25.9	2.0605	2.3022	2.4510	2.4699	2.6217
	30.8	1.0483	1.5909	1.8777	1.9985	2.1274
	35.8	0.4157	1.0925	1.2745	1.4028	1.6543
	40.8	0.3572	0.7653	0.9657	1.0359	1.2423
	45.9	-0.1074	0.3471	0.4584	0.6013	0.9278
	50.8	-0.2827	0.0172	0.2680	0.2907	0.4220
	55.9	-0.5163	-0.3175	-0.1771	-0.0864	0.0863
	61.1	-0.7259	-0.6200	-0.4795	-0.4348	-0.2624
$\overline{C}_{L_q}$	20.8	0.6274	-0.6749	-0.4411	-0.4391	0.1617
	25.9	6.8878	2.8420	1.3282	0.5986	0.4959
	30.8	13.4790	6.8415	3.5802	2.3319	1.0400
	35.8	17.0380	7.8742	4.5156	3.2101	1.4278
	40.8	18.0300	7.8265	4.2304	2.9332	1.4082
	45.9	10.8080	5.3759	3.5004	2.2017	1.2853
	50.8	7.3799	3.6589	2.0937	1.2329	0.6319
	55.9	4.0848	2.6166	1.5641	1.0655	0.2893
	61.1	3.5036	1.7856	1.3260	1.0968	0.2086

Table V. In-phase and out-of-phase components of lift coefficient.

Component	α, deg	k = .081	k = .135	k = .190	k = .237	k = .397
$\overline{C}_{N_\alpha}$	20.8	3.2712	3.2778	3.2707	3.2352	3.2971
	25.9	2.8836	3.1394	3.3009	3.3276	3.5424
	30.8	2.0690	2.6814	3.0051	3.1475	3.3558
	35.8	1.5553	2.3672	2.5946	2.7657	3.1757
	40.8	1.5905	2.1257	2.3880	2.5087	2.8960
	45.9	1.0970	1.7409	1.9091	2.1241	2.7033
	50.8	1.0552	1.5107	1.9158	1.9464	2.3034
	55.9	0.9679	1.3127	1.5457	1.7166	2.1429
	61.1	0.9027	1.1141	1.4076	1.5303	2.0425
$\overline{C}_{N_q}$	20.8	0.6466	-0.8186	-0.5106	-0.4904	0.1744
	25.9	7.4524	2.9259	1.3458	0.5894	0.5346
	30.8	15.0792	7.4842	3.9208	2.5651	1.1490
	35.8	20.4228	9.2855	5.3797	3.8608	1.7763
	40.8	23.1772	9.9533	5.4853	3.8410	1.9113
	45.9	15.4526	7.5281	4.9940	3.2200	1.8646
	50.8	11.8092	5.7557	3.3916	2.1095	1.2027
	55.9	7.4302	5.2961	2.7569	1.8374	0.6297
	61.1	8.0909	4.2358	2.3987	2.0903	0.3287

Table VI. In-phase and out-of-phase components of normal-force coefficient.

Component	α, deg	k = .081	k = .135	k = .190	k = .237	k = .397
$\overline{C}_{m_\alpha}$	20.8	0.5183	0.5096	0.5076	0.5013	0.4656
	25.9	0.4529	0.4775	0.4937	0.4941	0.5023
	30.8	0.1901	0.2764	0.3429	0.3668	0.3865
	35.8	0.1090	0.2378	0.2325	0.2419	0.2278
	40.8	0.1509	0.1682	0.1318	0.1336	0.0124
	45.9	0.0323	0.0706	0.0253	0.0458	-0.0816
	50.8	-0.0921	-0.0733	0.0041	0.0489	0.0633
	55.9	-0.1755	-0.1386	-0.1546	-0.0612	0.1958
	61.1	-0.2081	-0.1714	-0.1520	-0.1195	0.1636
$\overline{C}_{m_q}$	20.8	-0.8553	-1.1161	-1.0749	-1.0589	-1.0527
	25.9	-0.1240	-0.7076	-0.8825	-0.9682	-1.0761
	30.8	1.7197	0.4942	-0.1789	-0.2611	-0.7195
	35.8	2.3630	0.5519	-0.3245	-0.4752	-0.7640
	40.8	1.3537	-0.3968	-0.7955	-0.7878	-0.6640
	45.9	-0.1715	-0.5400	-0.4869	-0.6901	-0.6076
	50.8	0.3532	-0.0418	0.0527	-0.1078	-0.4099
	55.9	0.0235	0.1021	0.1407	0.1023	-0.2927
	61.1	-0.0310	0.0538	0.0567	0.2266	0.0463

Table VII. In-phase and out-of-phase components of pitching-moment coefficient.

Measured Data	Standard Error			
	$s(\hat{a})$		$s(C_{A_a}(\infty))^*$	
	min	max	min	max
$\overline{C}_{L_\alpha}$	0.056	0.074	0.13	0.15
$\overline{C}_{L_q}$			0.19	0.21
$\overline{C}_{N_\alpha}$	0.091	0.12	0.21	0.25
$\overline{C}_{N_q}$			0.30	0.34
$\overline{C}_{m_\alpha}$	0.034	0.14	0.069	0.17
$\overline{C}_{m_q}$			0.090	0.11

* for index $A_a = L_\alpha, L_q, N_\alpha, N_q, m_\alpha$, or m_q

Table VIII. Minimum and maximum values of standard errors of estimated parameters.

Measured Data	Parameter		
	τ_1	b_1, sec^{-1}	T_1, sec
$\overline{C}_{L_\alpha}, \overline{C}_{L_q}$	17.2 ± 1.0*	2.71 ± 0.16	0.368 ± 0.023
$\overline{C}_{N_\alpha}, \overline{C}_{N_q}$	17.1 ± 1.3	2.73 ± 0.21	0.365 ± 0.028
$\overline{C}_{m_\alpha}, \overline{C}_{m_q}$	25.1 ± 8.7	1.86 ± 0.64	0.540 ± 0.190

* the second value indicates the standard error

Table IX. Estimated and computed parameters.

Parameter	C_L		C_N	
	$\hat{\theta}$	$s(\hat{\theta})$	$\hat{\theta}$	$s(\hat{\theta})$
θ_0	16.0	1.4	16.0	2.1
θ_1	-48.4	4.8	-46.4	7.1
θ_2	33.6	3.8	32.4	5.7
θ_3	-50.9	11.3	-44.6	16.9
θ_4	-2.0	1.7	-2.6	2.5
θ_5	5.7	3.9	7.2	5.8
θ_6	-3.4	2.7	-4.1	4.0
θ_7	12.1	0.51	13.8	0.75
θ_8	-46.2	1.7	-51.8	2.5
θ_9	35.7	1.3	38.9	1.9
θ_{10}	-57.8	3.4	-59.5	5.0

Table X. Estimated parmeters and their standard errors in Model II for measured lift and normal-force coefficients.

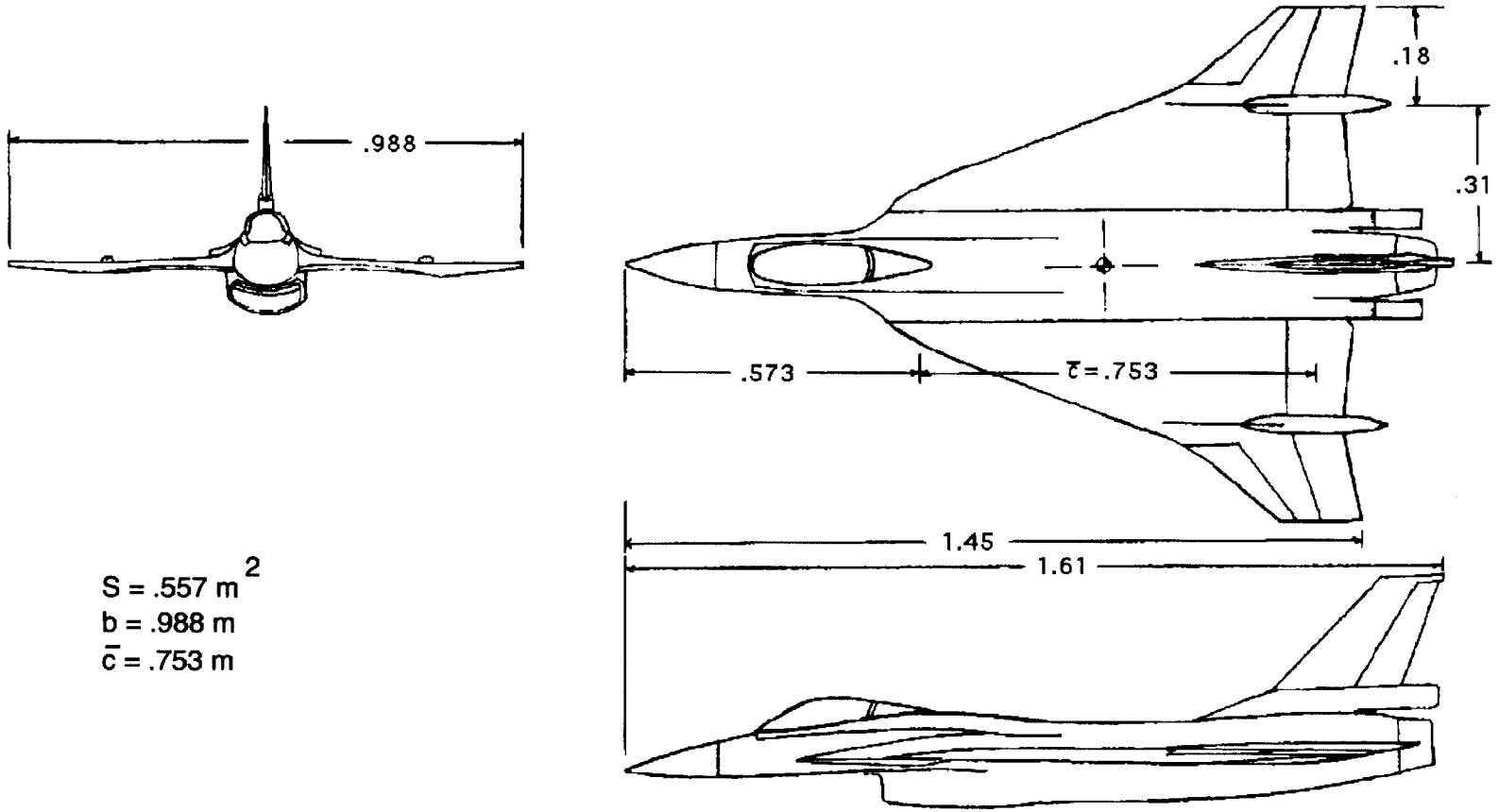

Figure 1. Three-view sketch of F-16XL model.

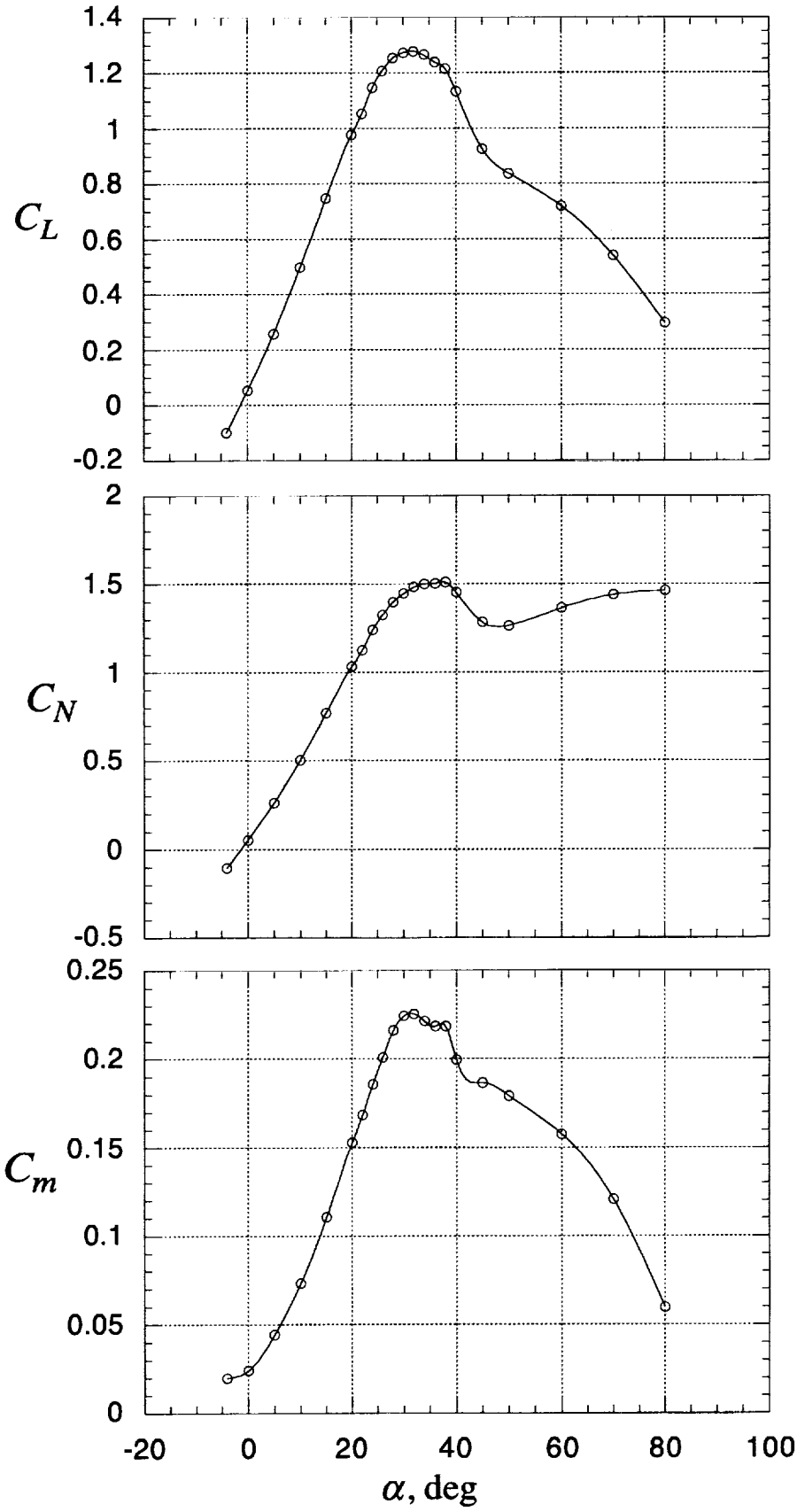

Figure 2. Variation of longitudinal coefficients with angle of attack. $\beta=0°$, $\delta_e=0°$.

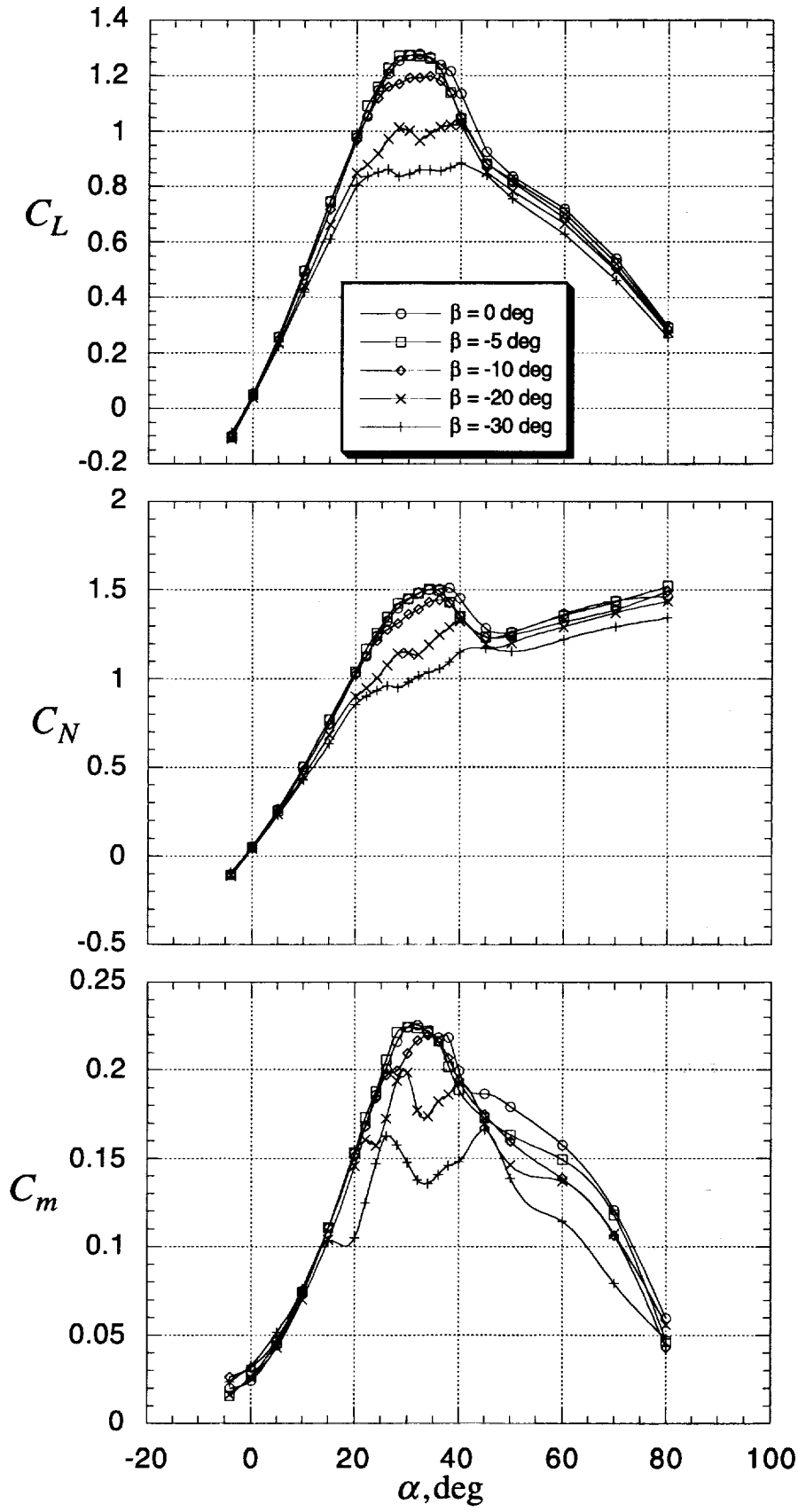

Figure 3. Effect of sideslip on longitudinal coefficients. δ_e=0°.

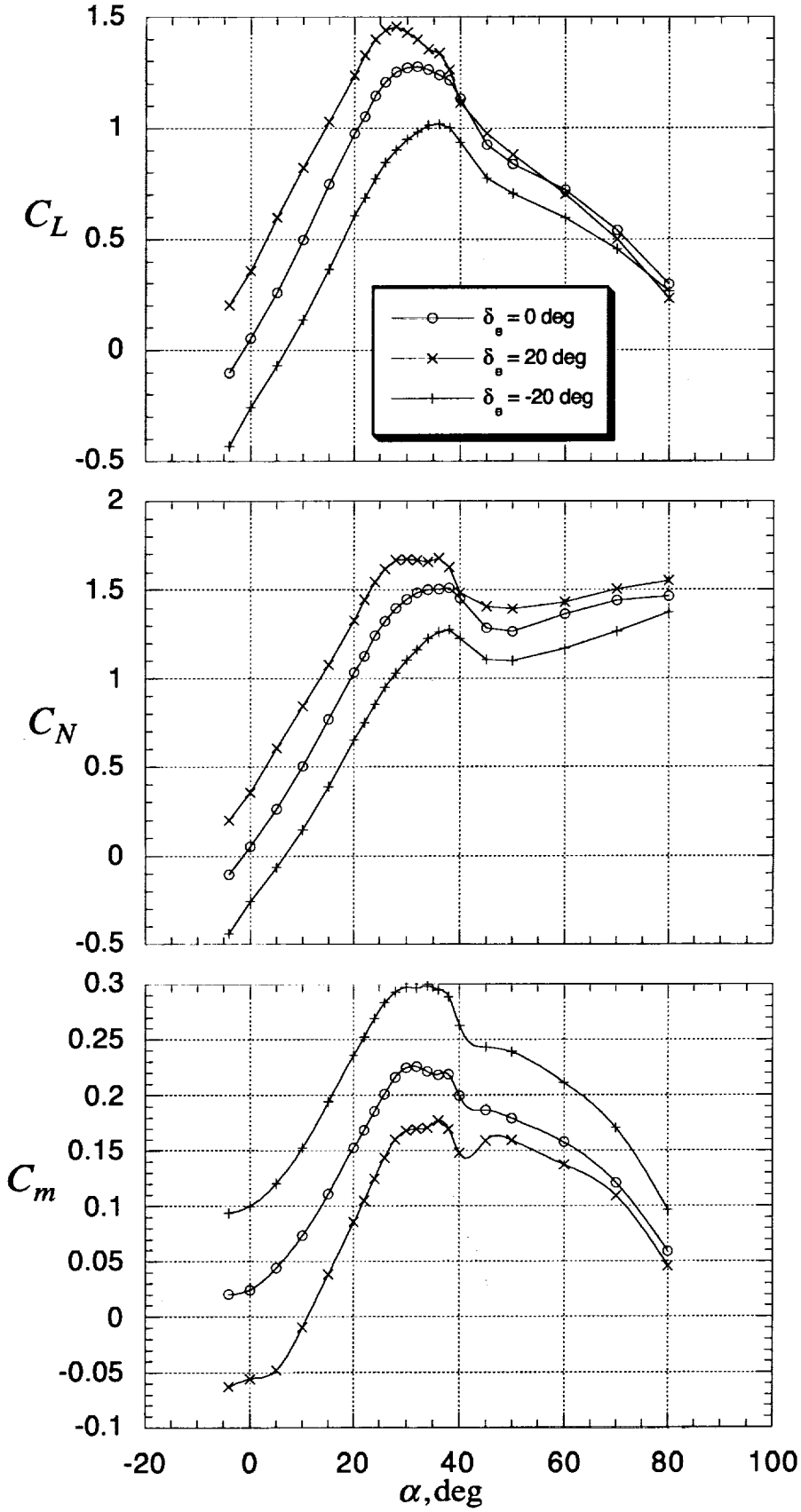

Figure 4. Effect of elevon and flaperon deflection on longitudinal coefficients. β=0°.

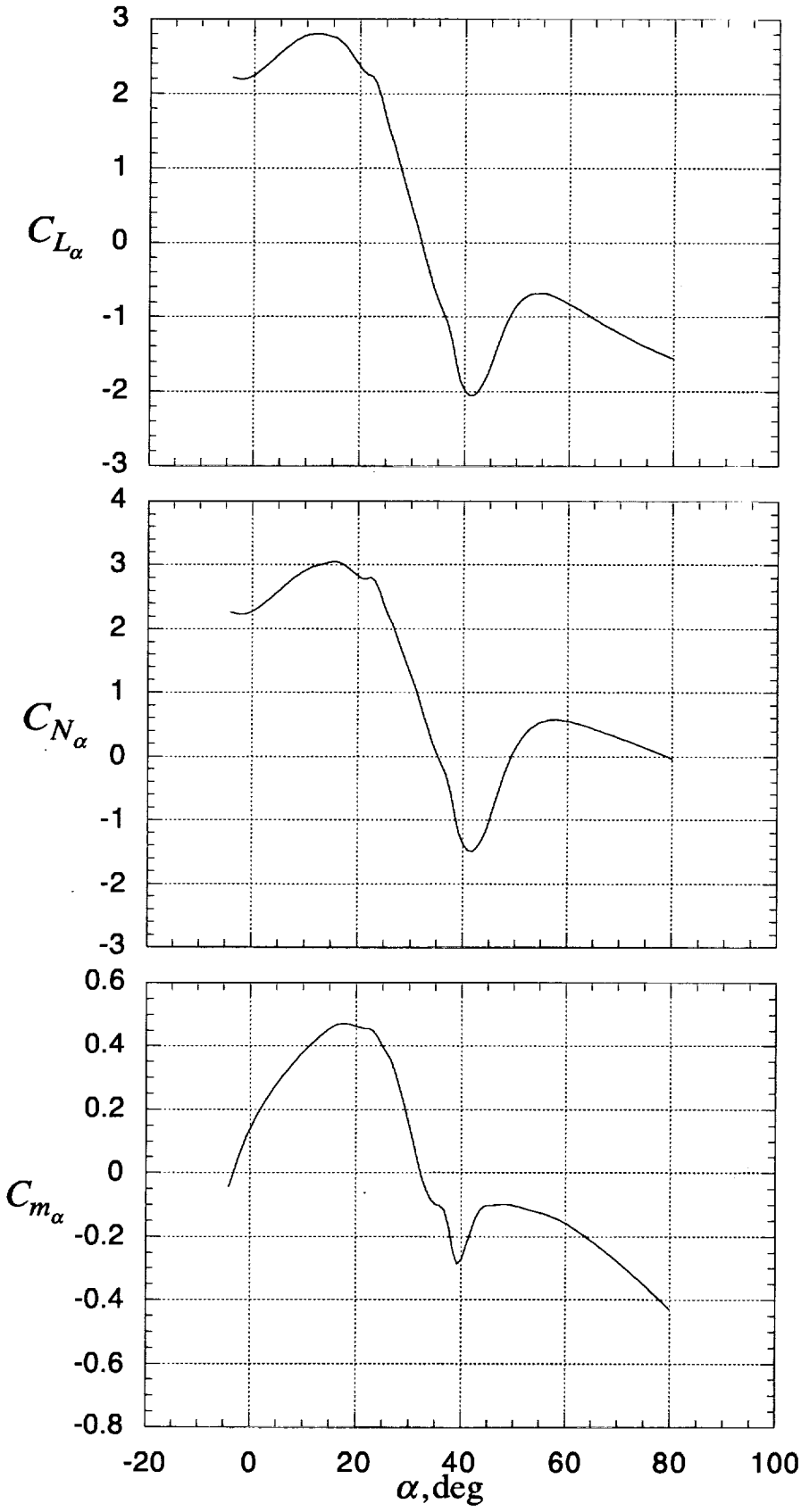

Figure 5. Variation of stability parameters with angle of attack.

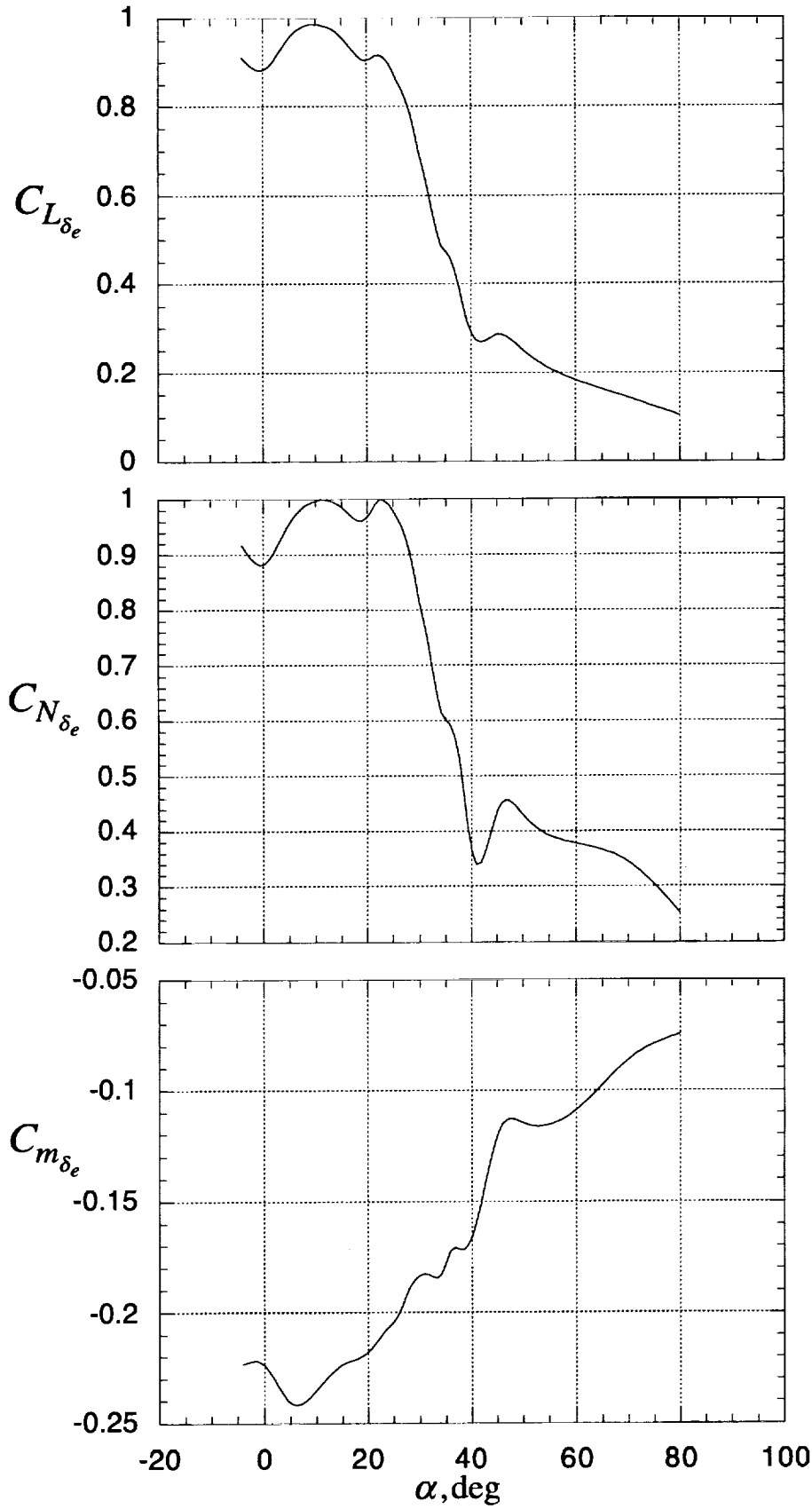

Figure 6 . Variation of control effectiveness with angle of attack.

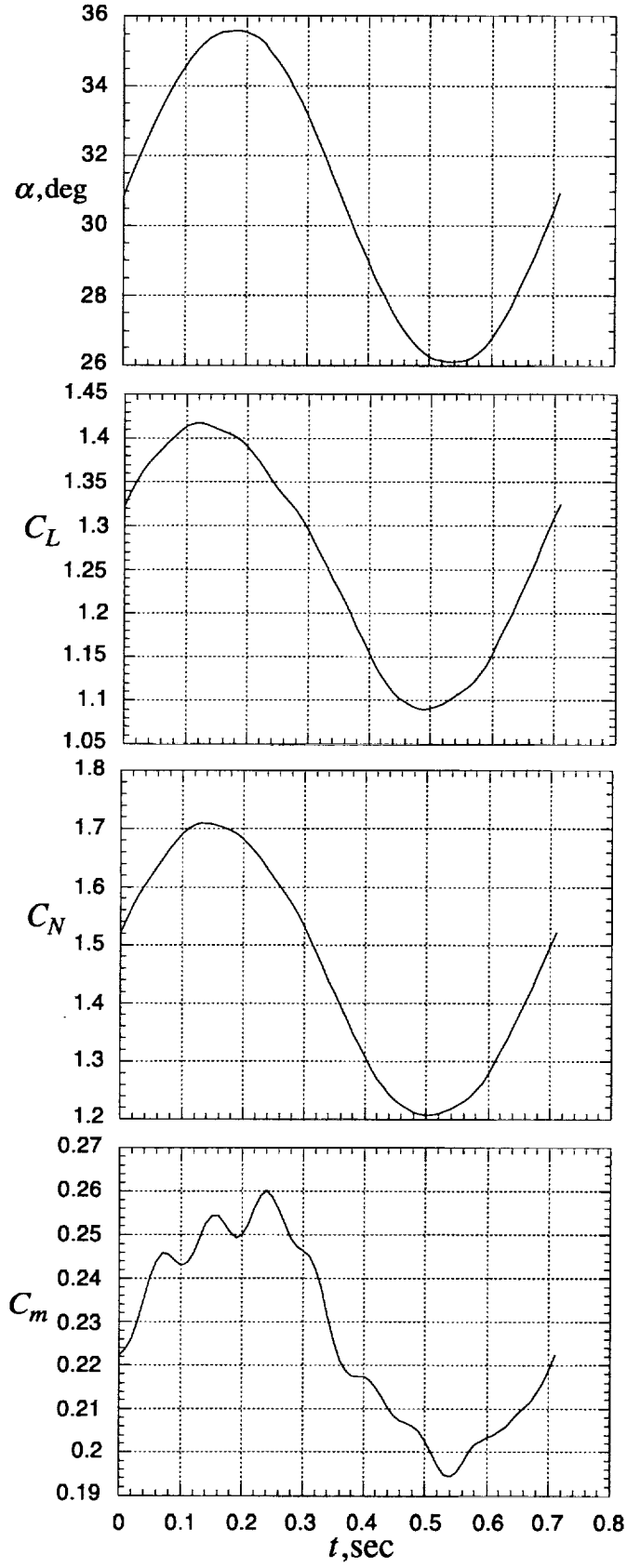

Figure 7. Variation of angle of attack and longitudinal coefficients with time. k=.190, α_o=30.8°.

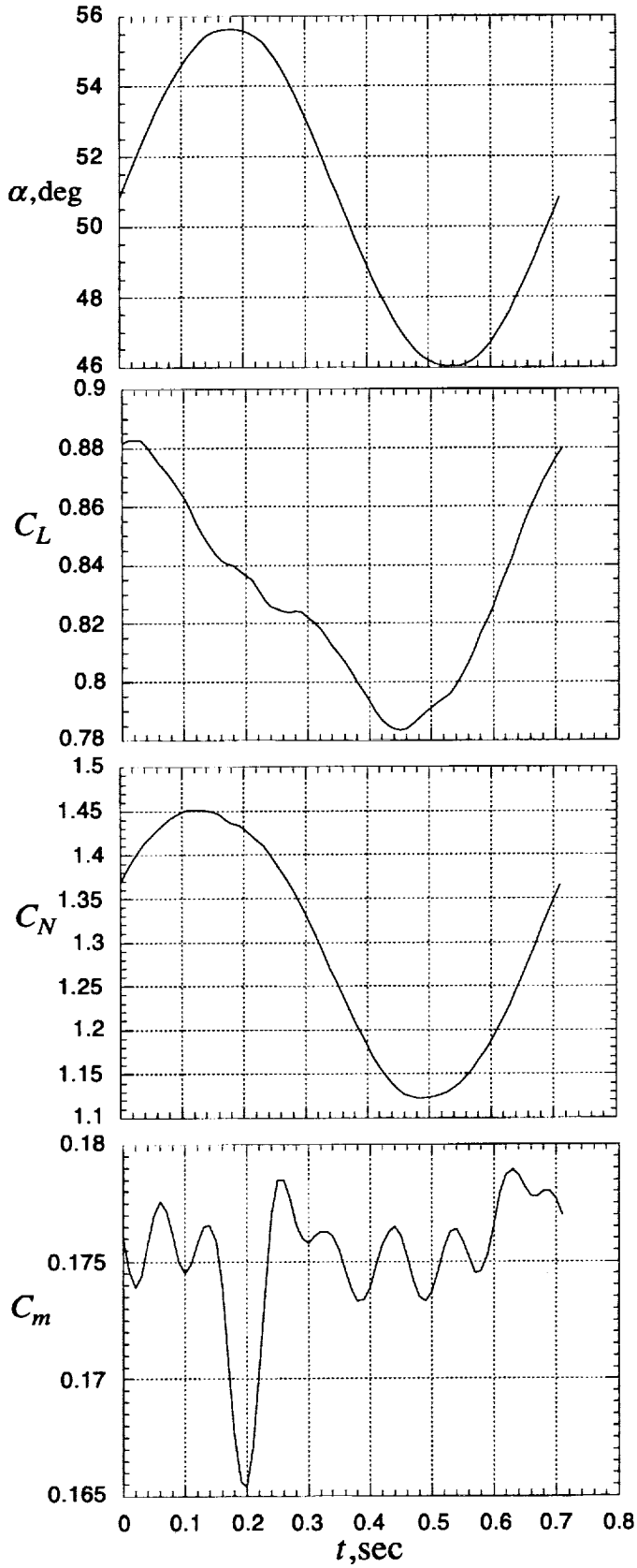

Figure 8. Variation of angle of attack and longitudinal coefficients with time. k=.190, α_o=50.8°.

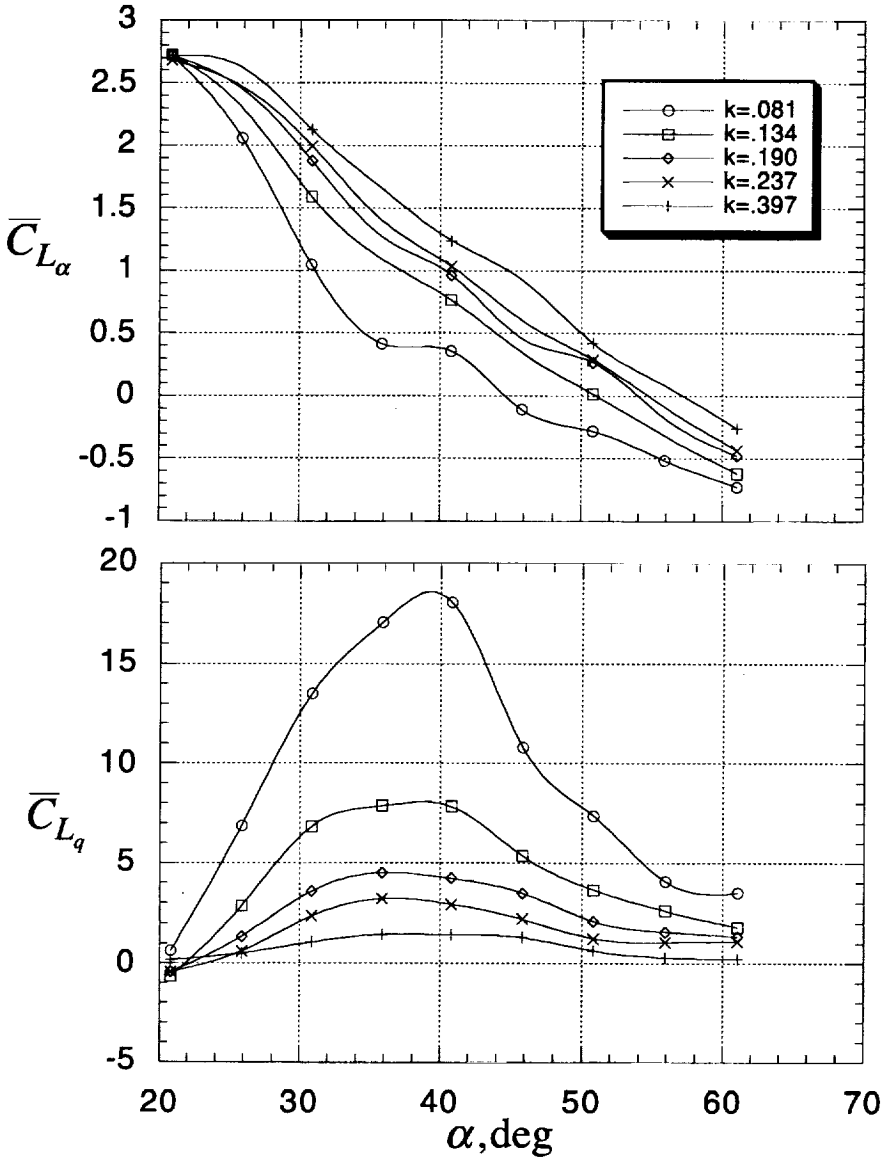

Figure 9. Variation of in-phase and out-of-phase components with angle of attack for different values of reduced frequency.

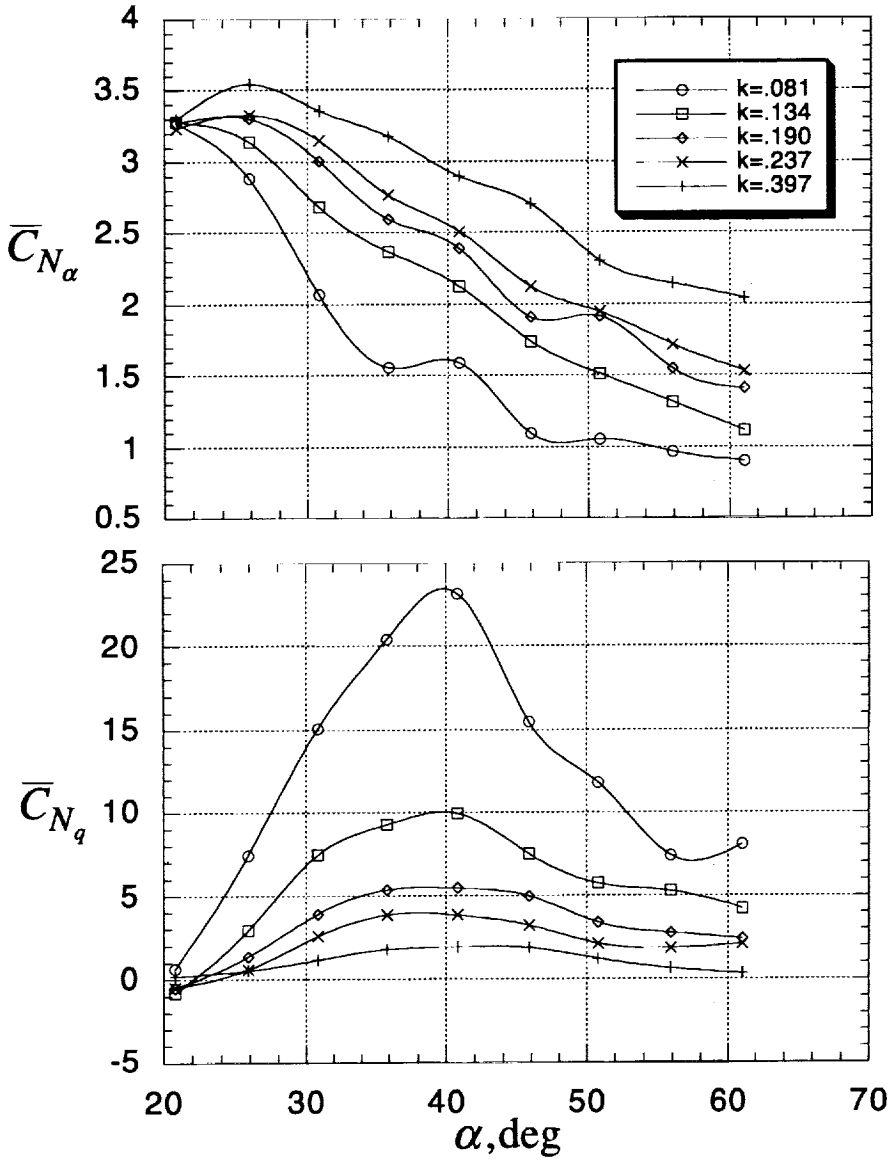

Figure 9. Continued.

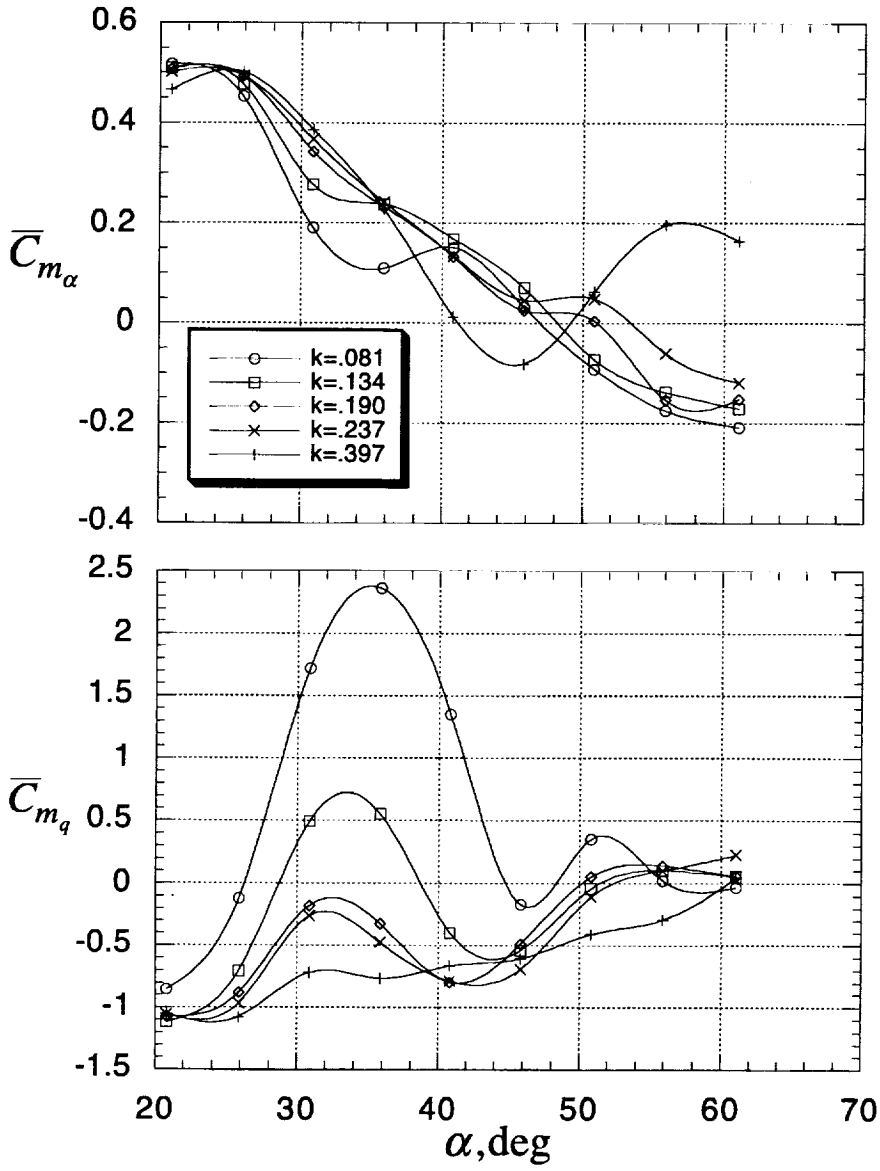

Figure 9. Concluded.

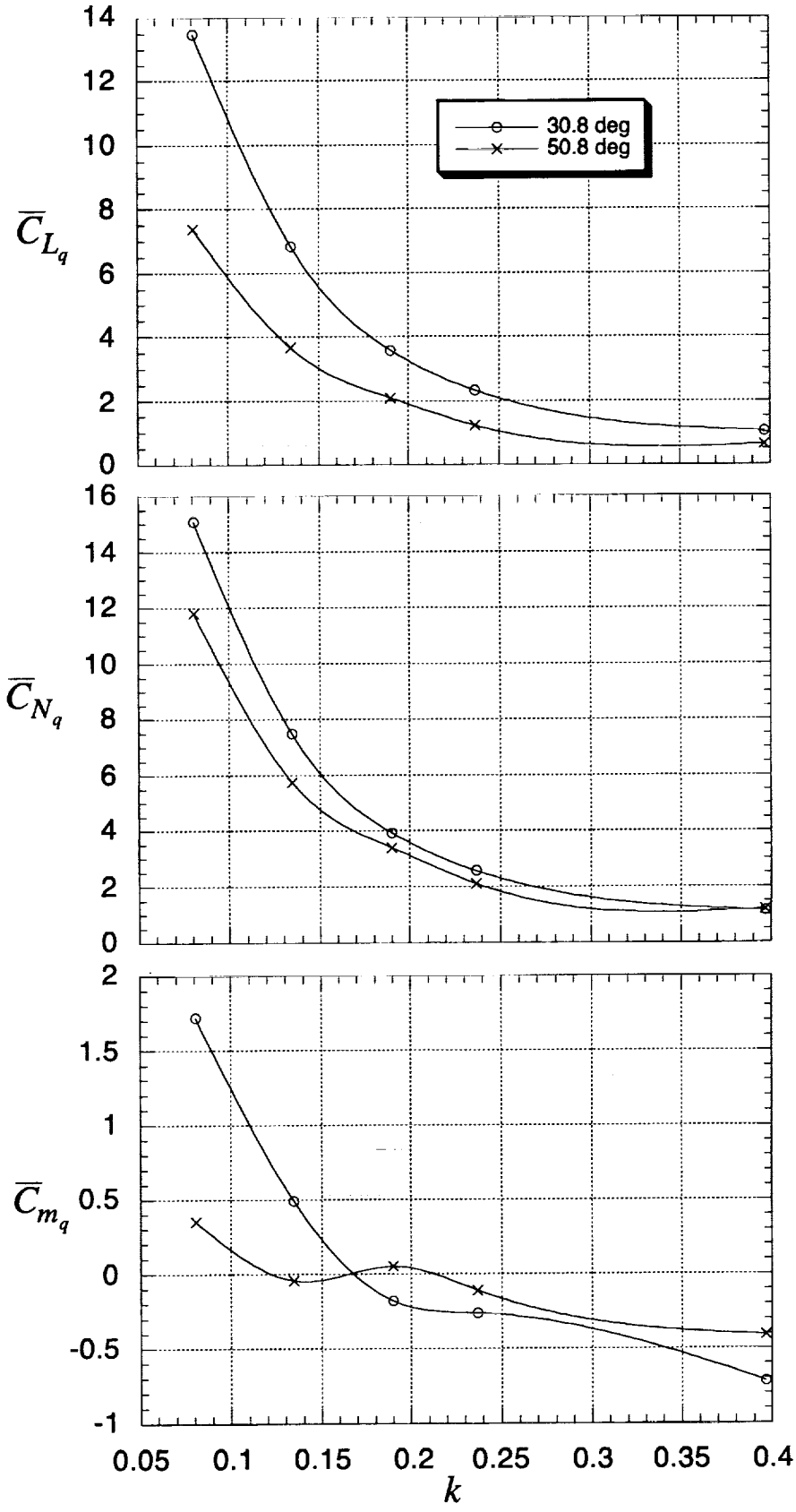

Figure 10. Variation of out-of-phase components with reduced frequency.

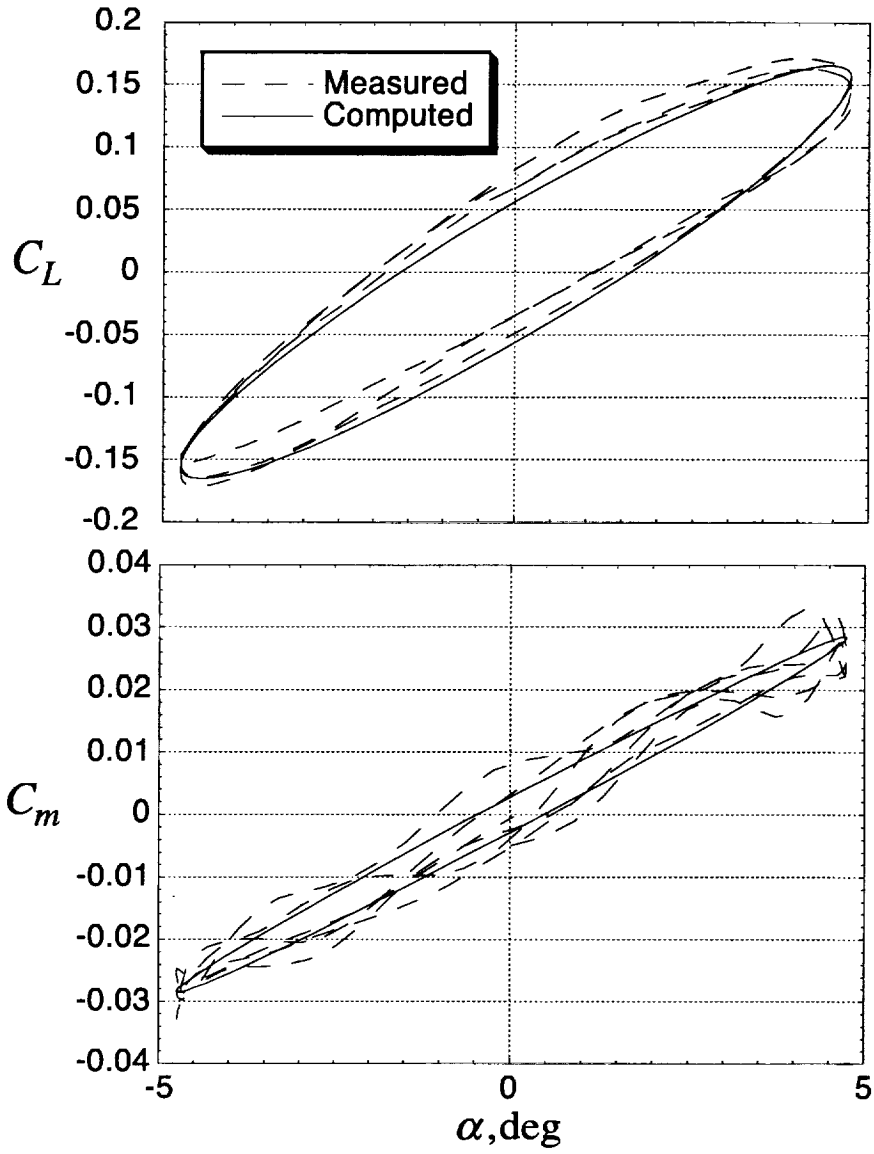

Figure 11. Comparison of measured and predicted values of C_L and C_m. k=.190, α_o=30.8°.

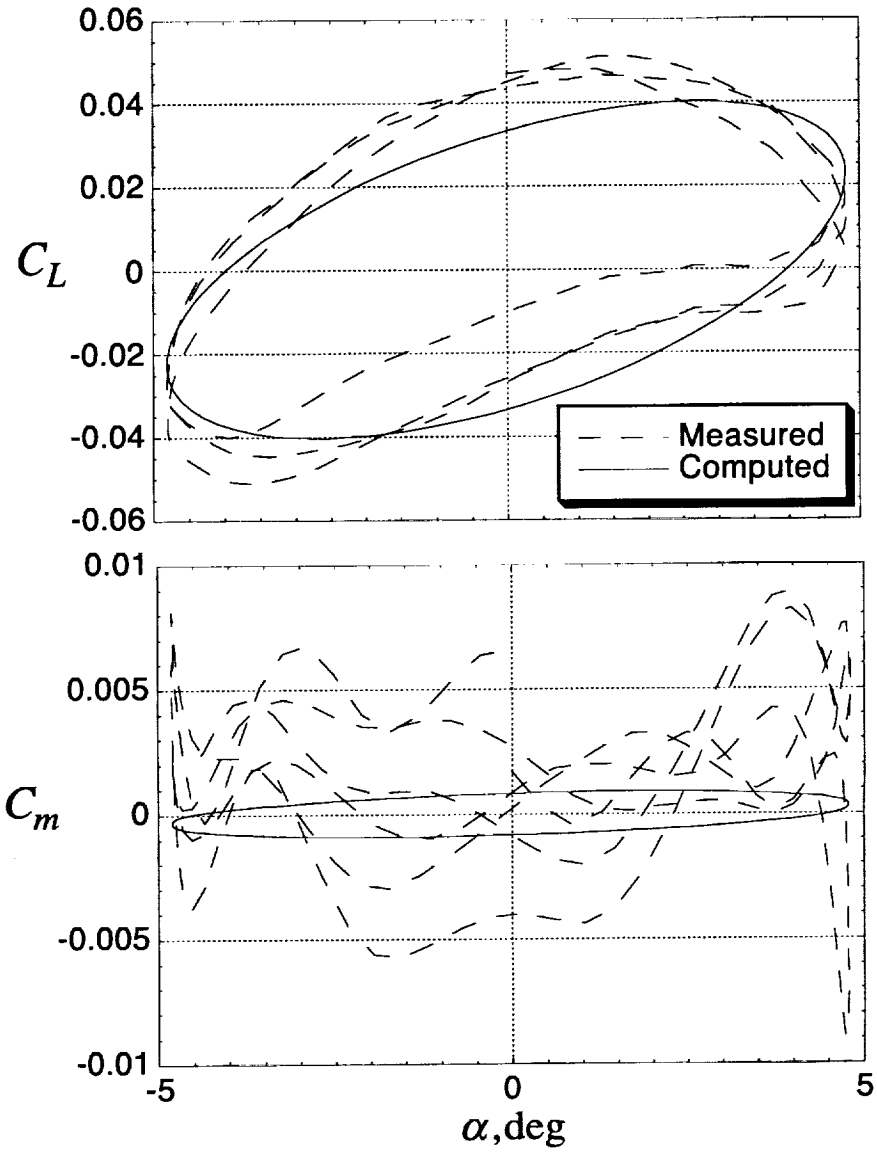

Figure 12. Comparison of measured and predicted values of C_L and C_m. k=.190, α_o=50.8°.

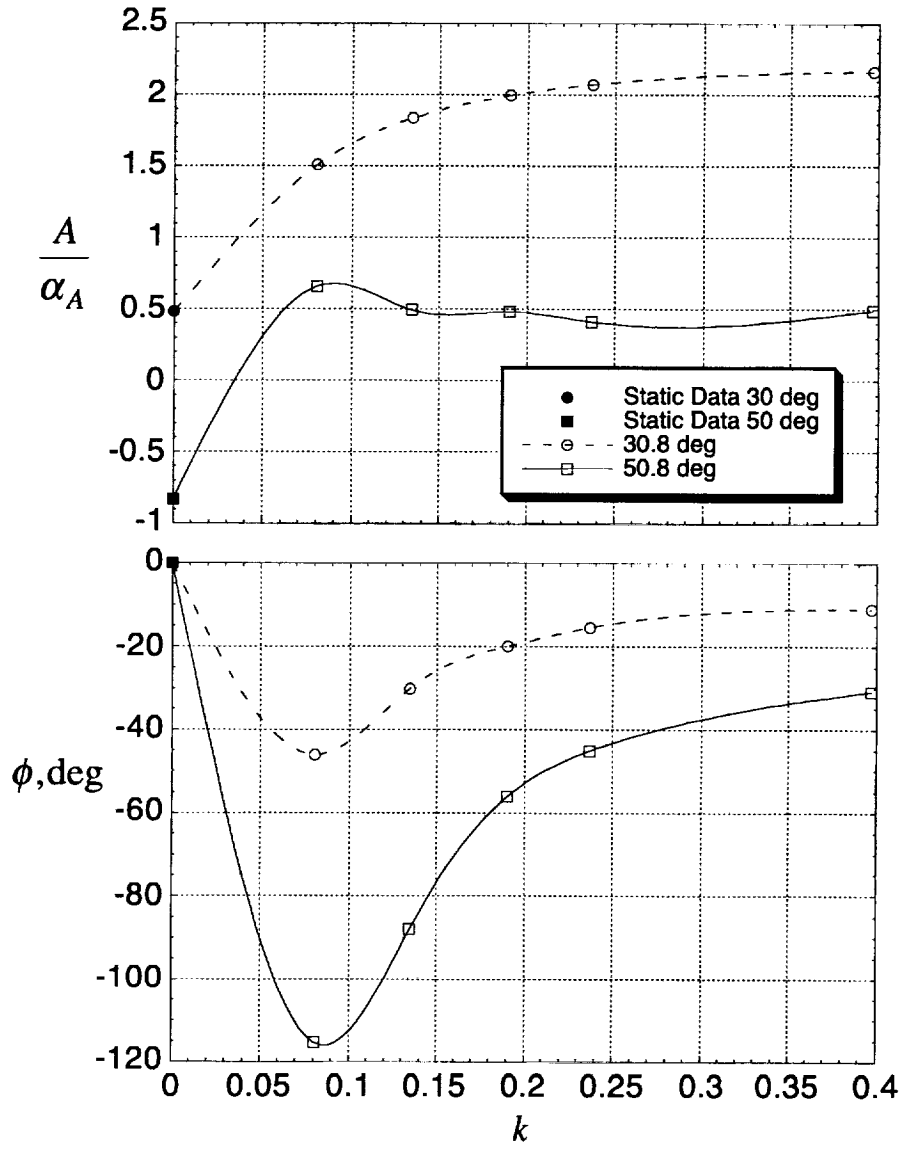

Figure 13. Amplitude and phase characteristics of C_L/α transfer function.

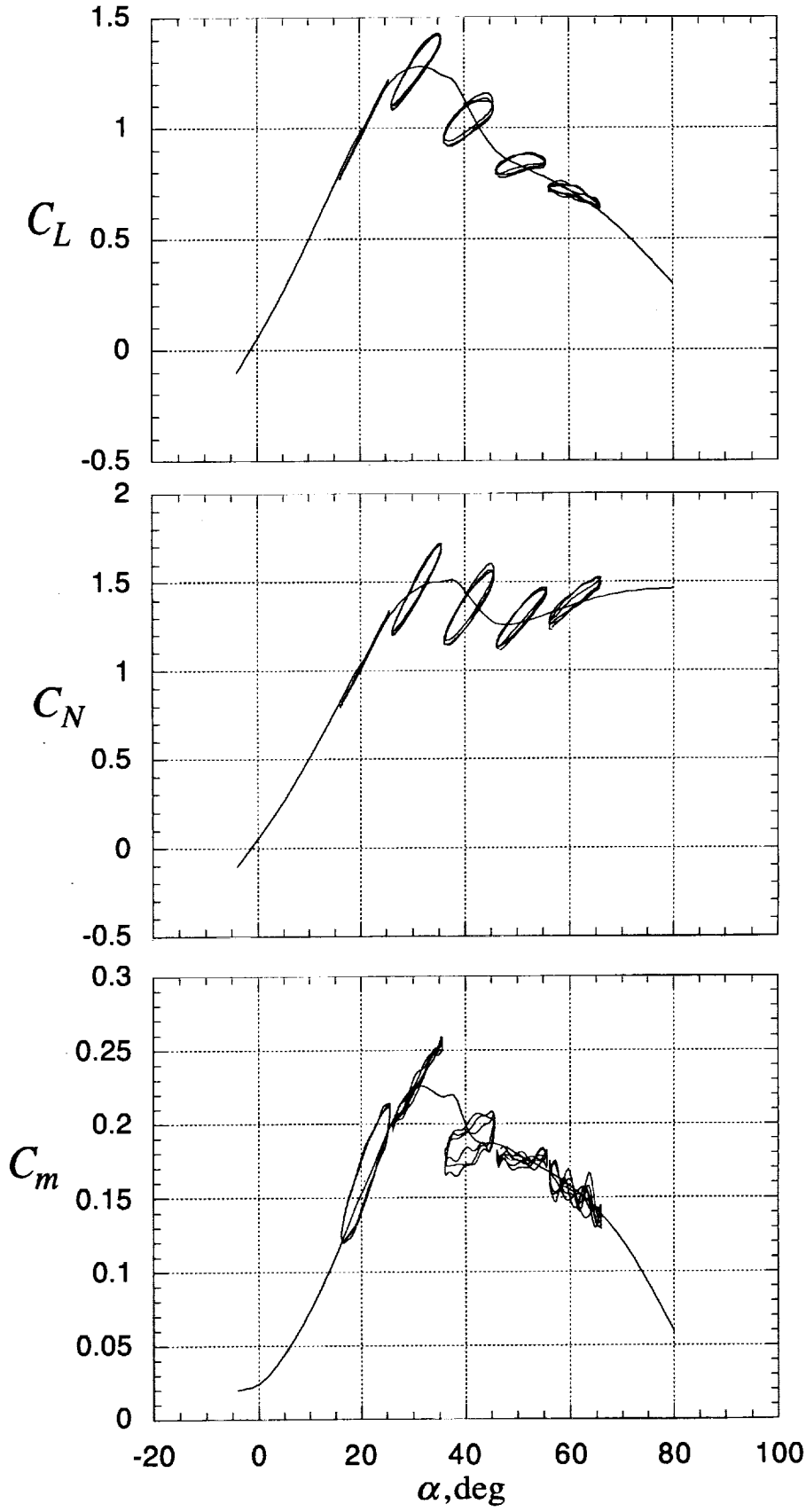

Figure 14. Longitudinal coefficients obtained from static and oscillatory data for k=.190.

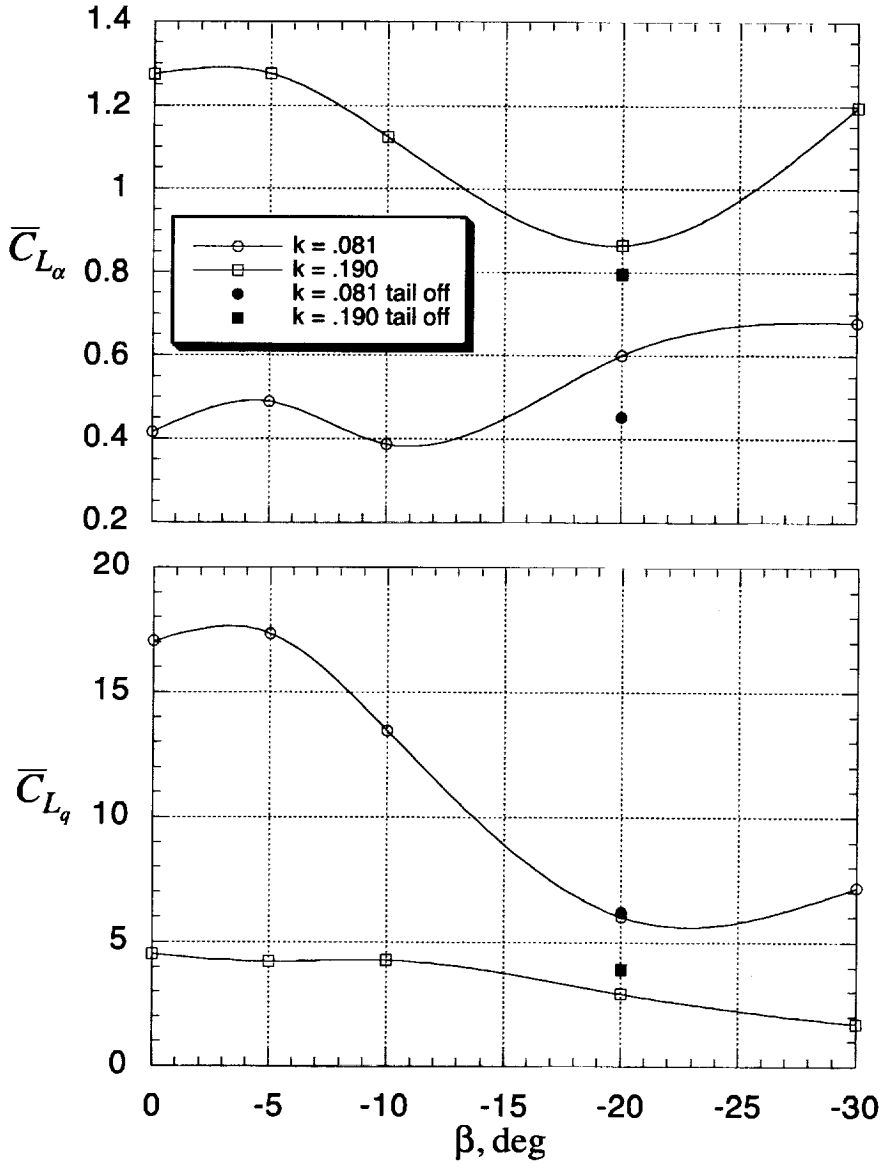

Figure 15. Variation of in-phase and out-of-phase components with sideslip angle.

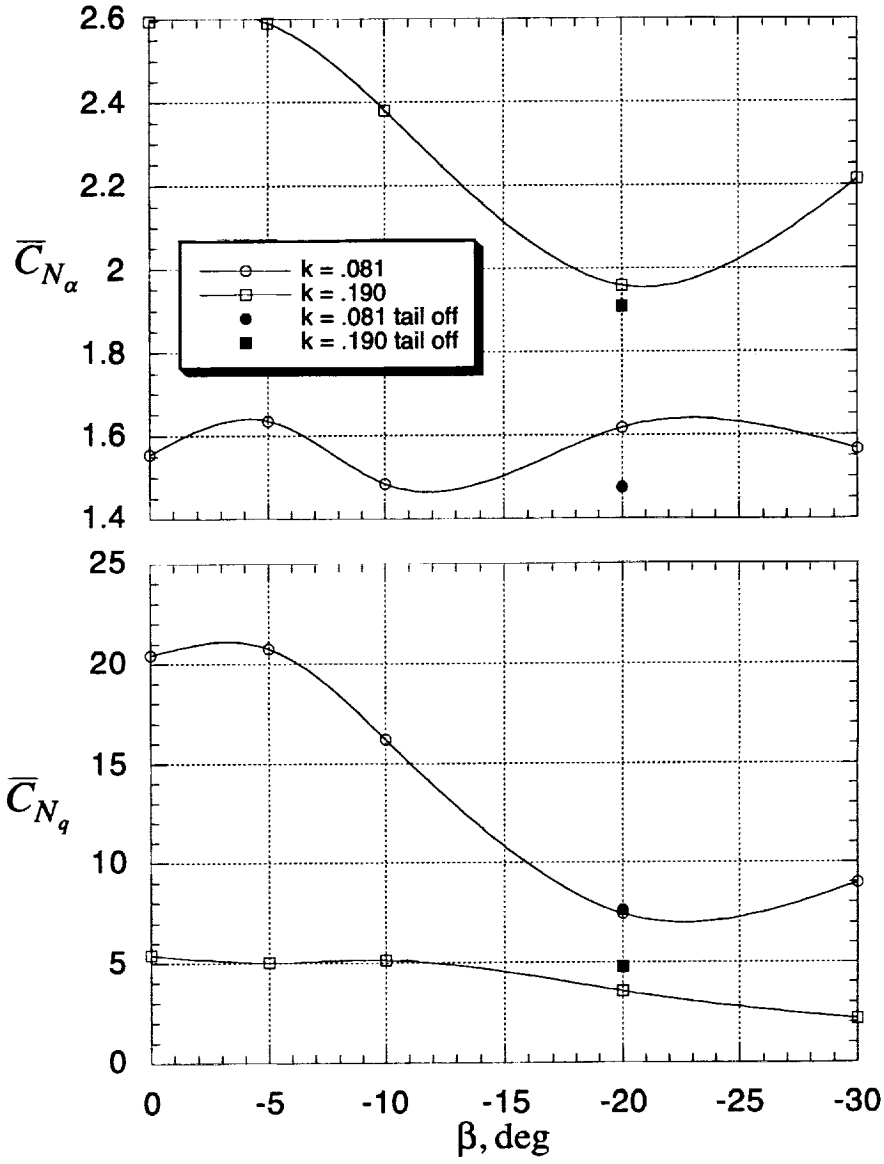

Figure 15. Continued.

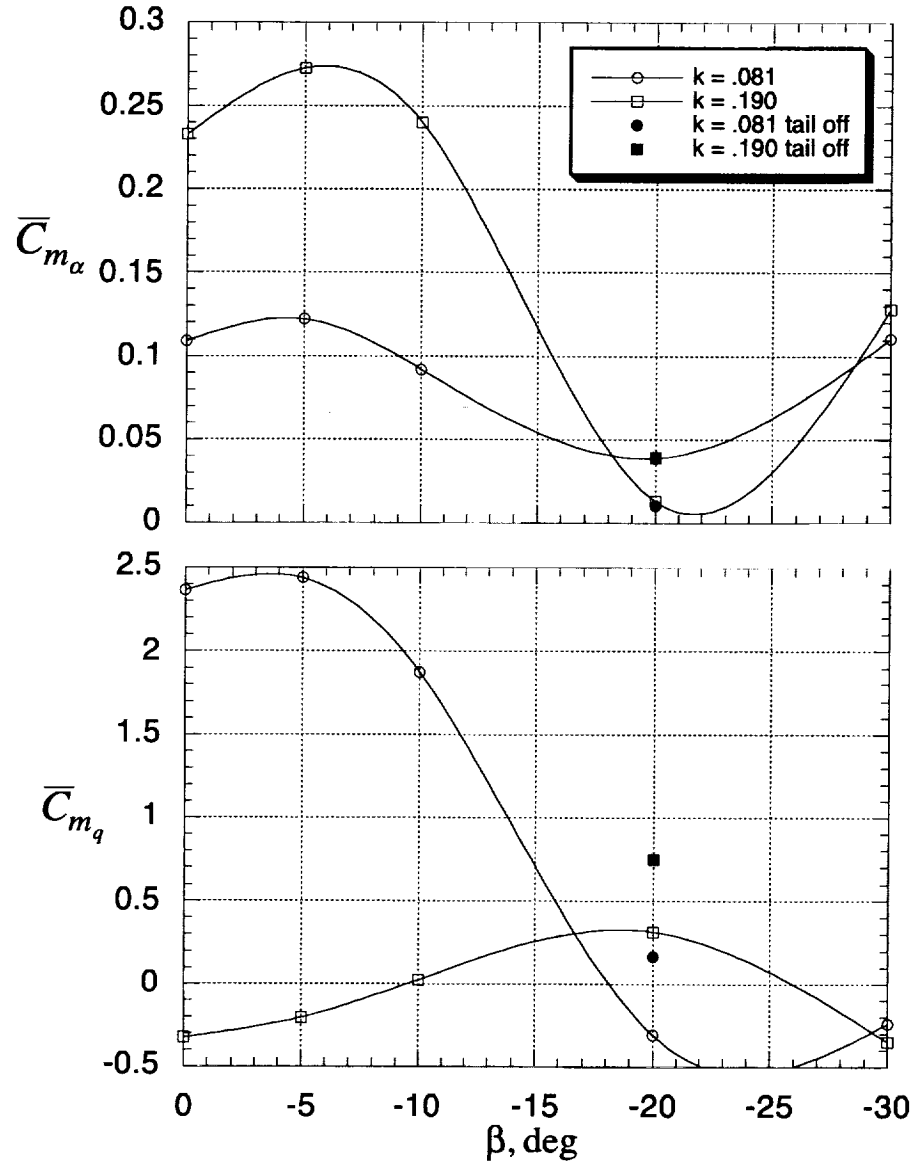

Figure 15. Concluded.

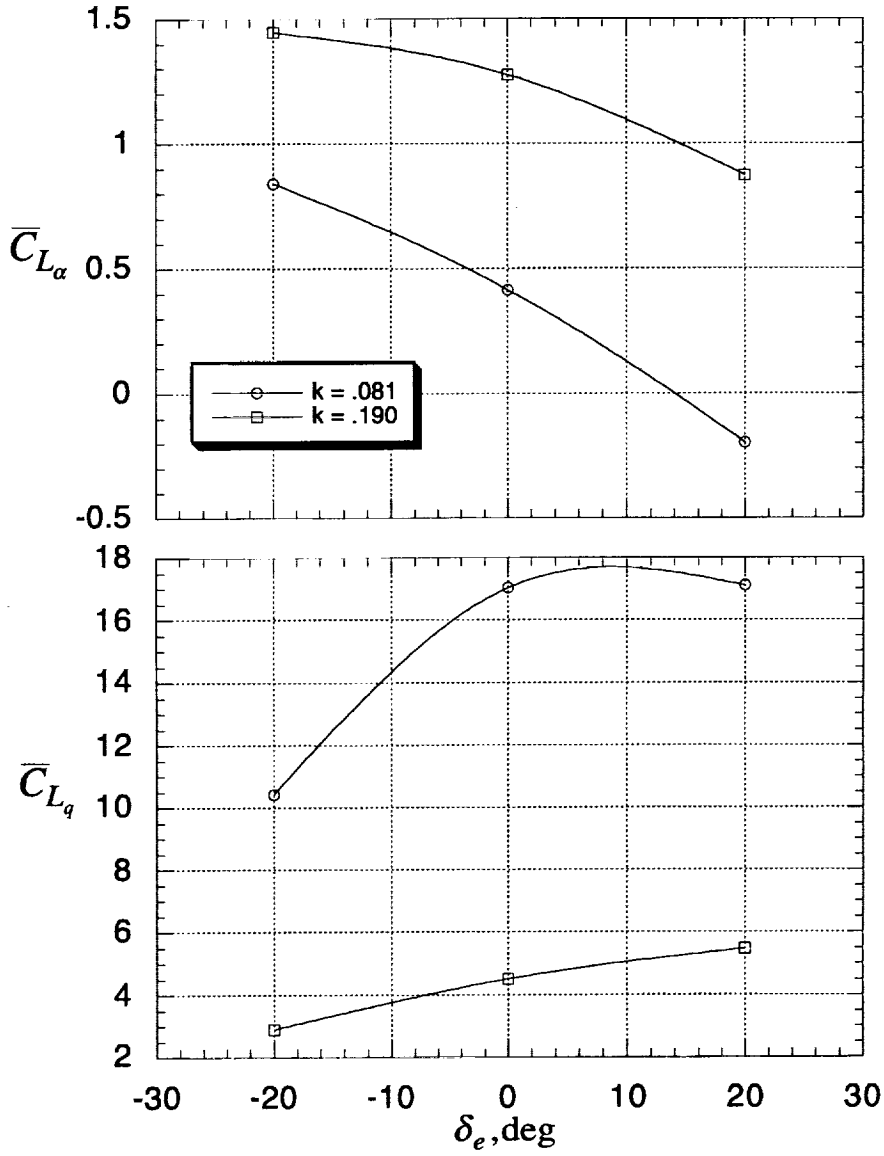

Figure 16. Variation of in-phase and out-of-phase components with elevon/flaperon. α_o=35.8°.

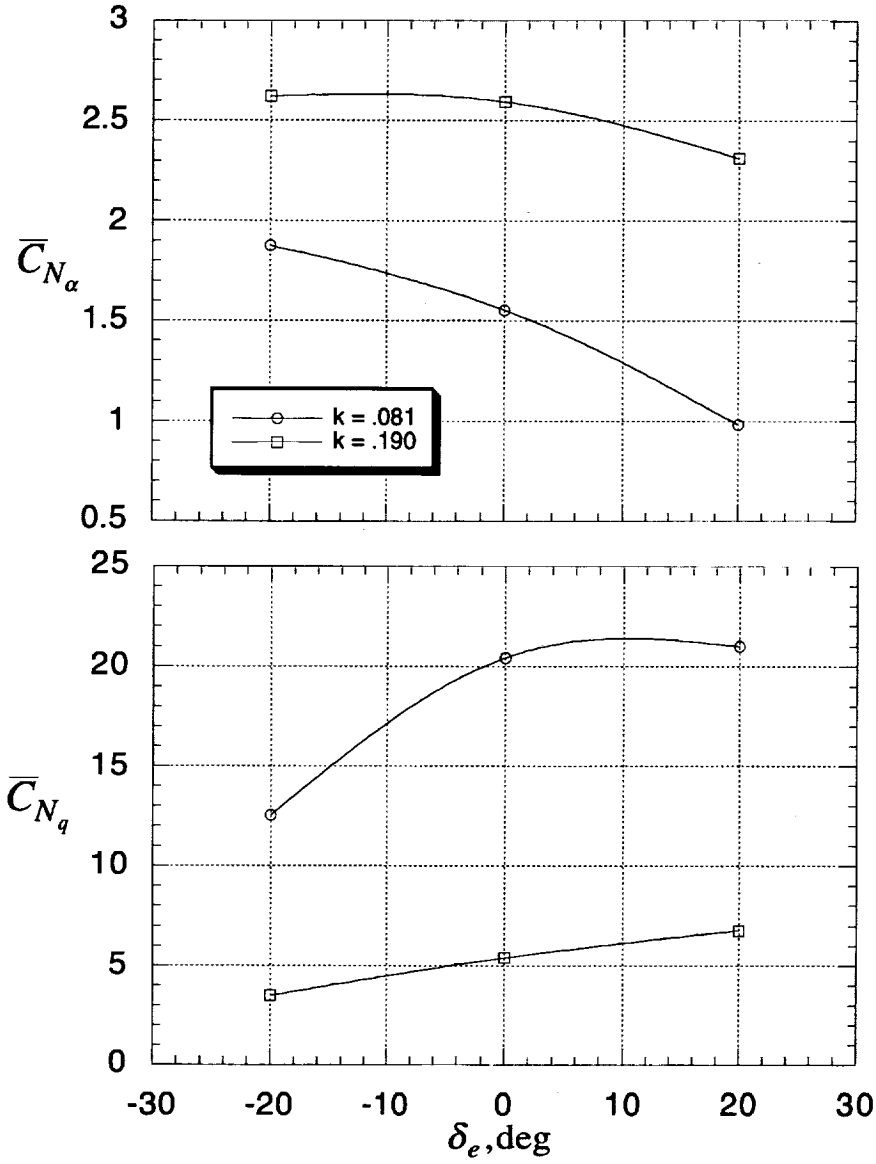

Figure 16. Continued.

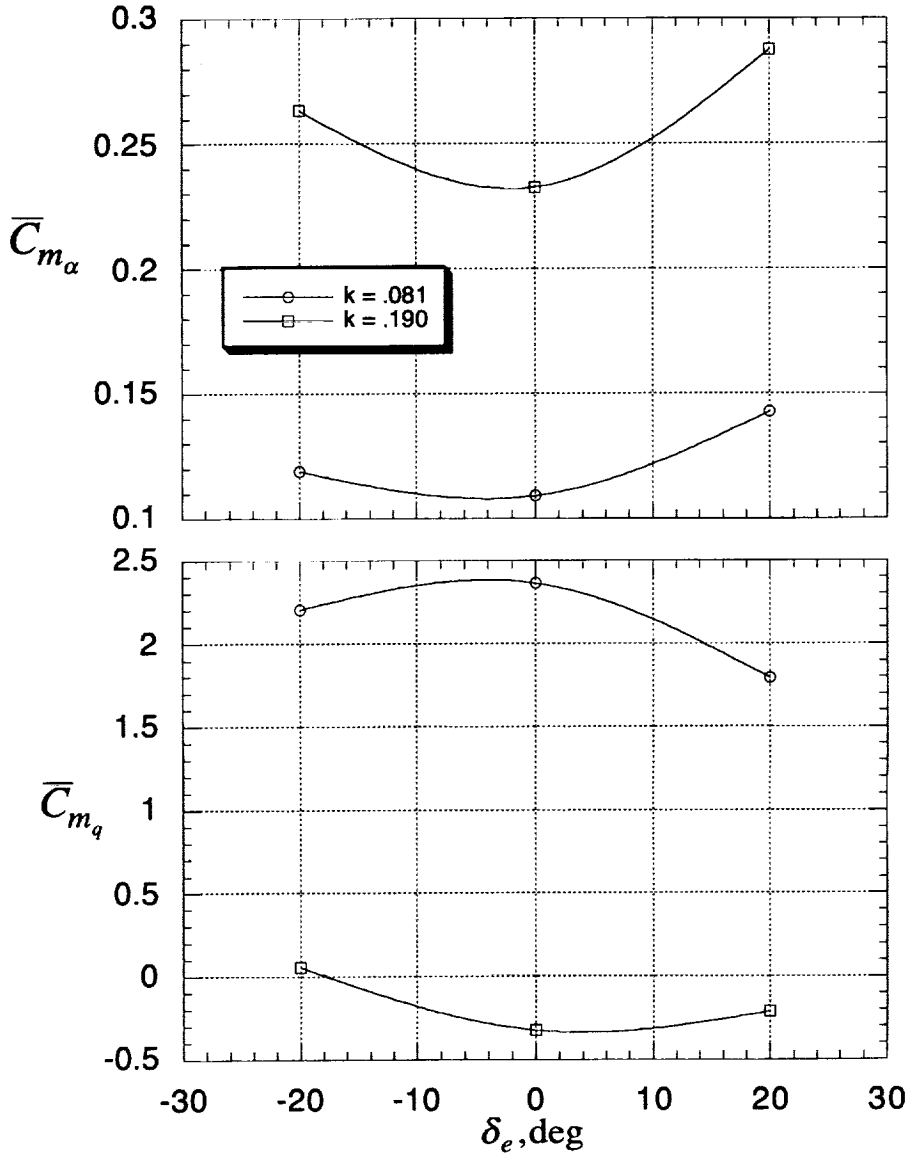

Figure 16. Concluded.

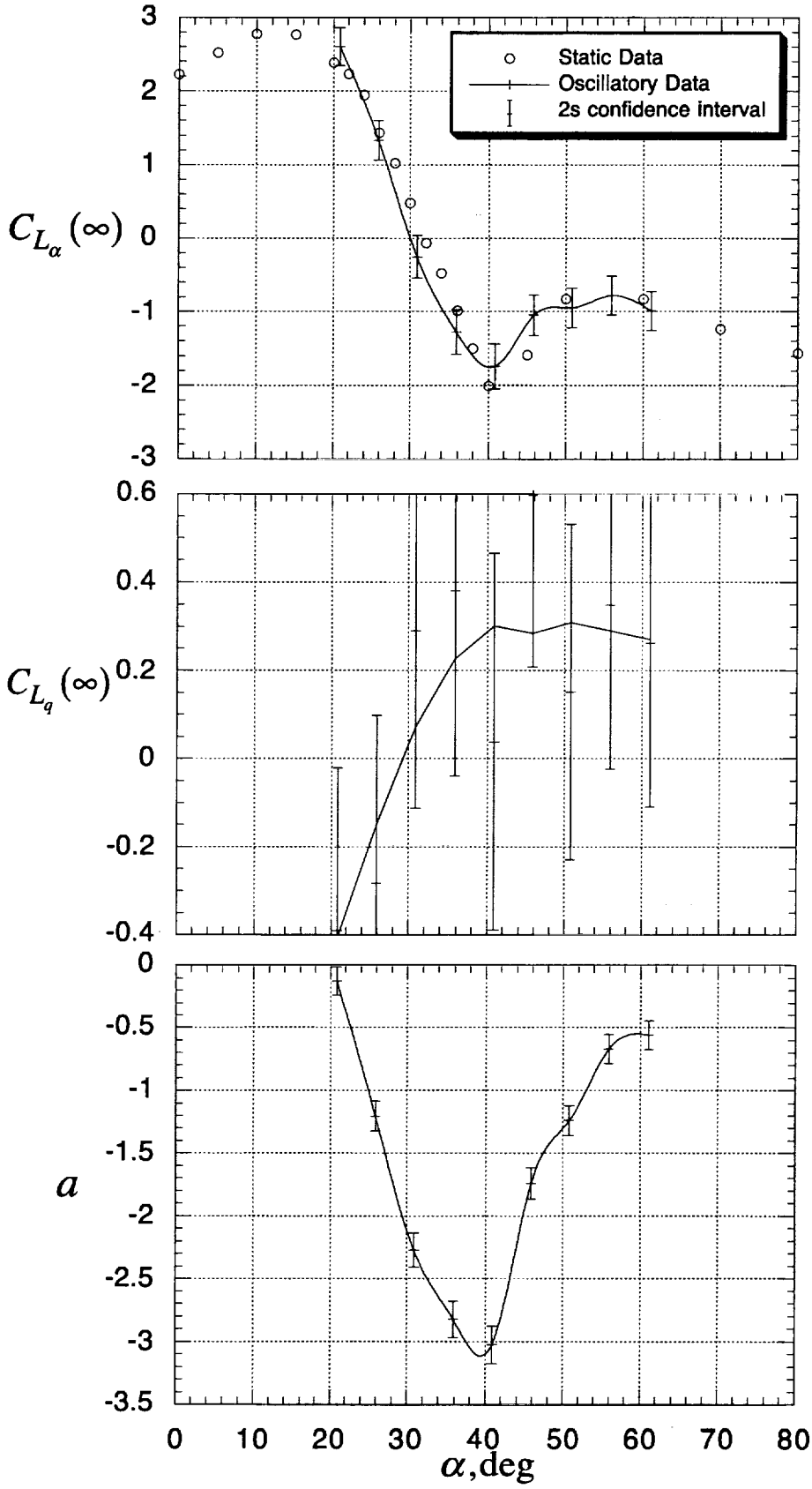

Figure 17. Estimated parameters of lift components. Model I.

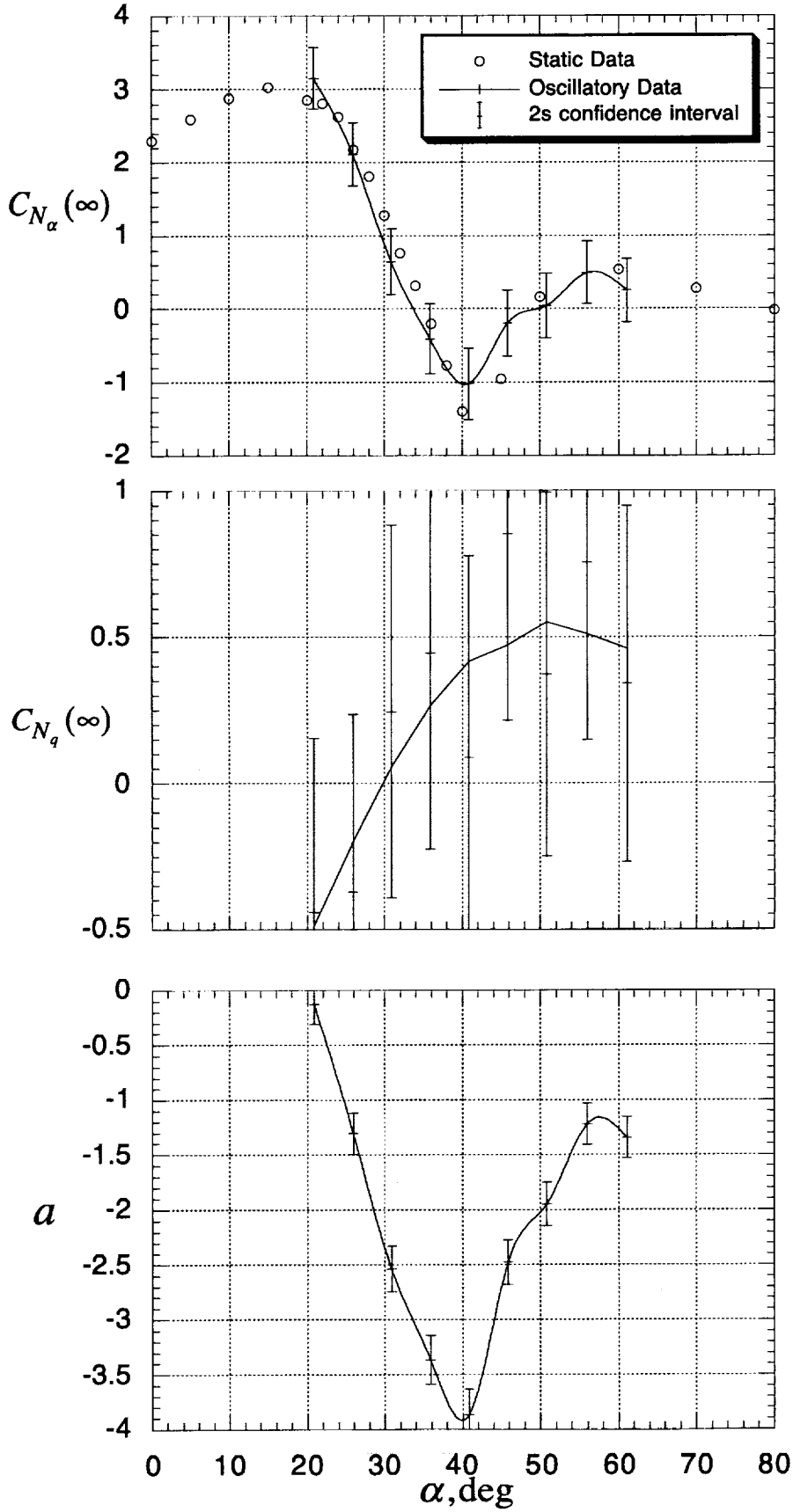

Figure 18. Estimated parameters of normal-force components. Model I.

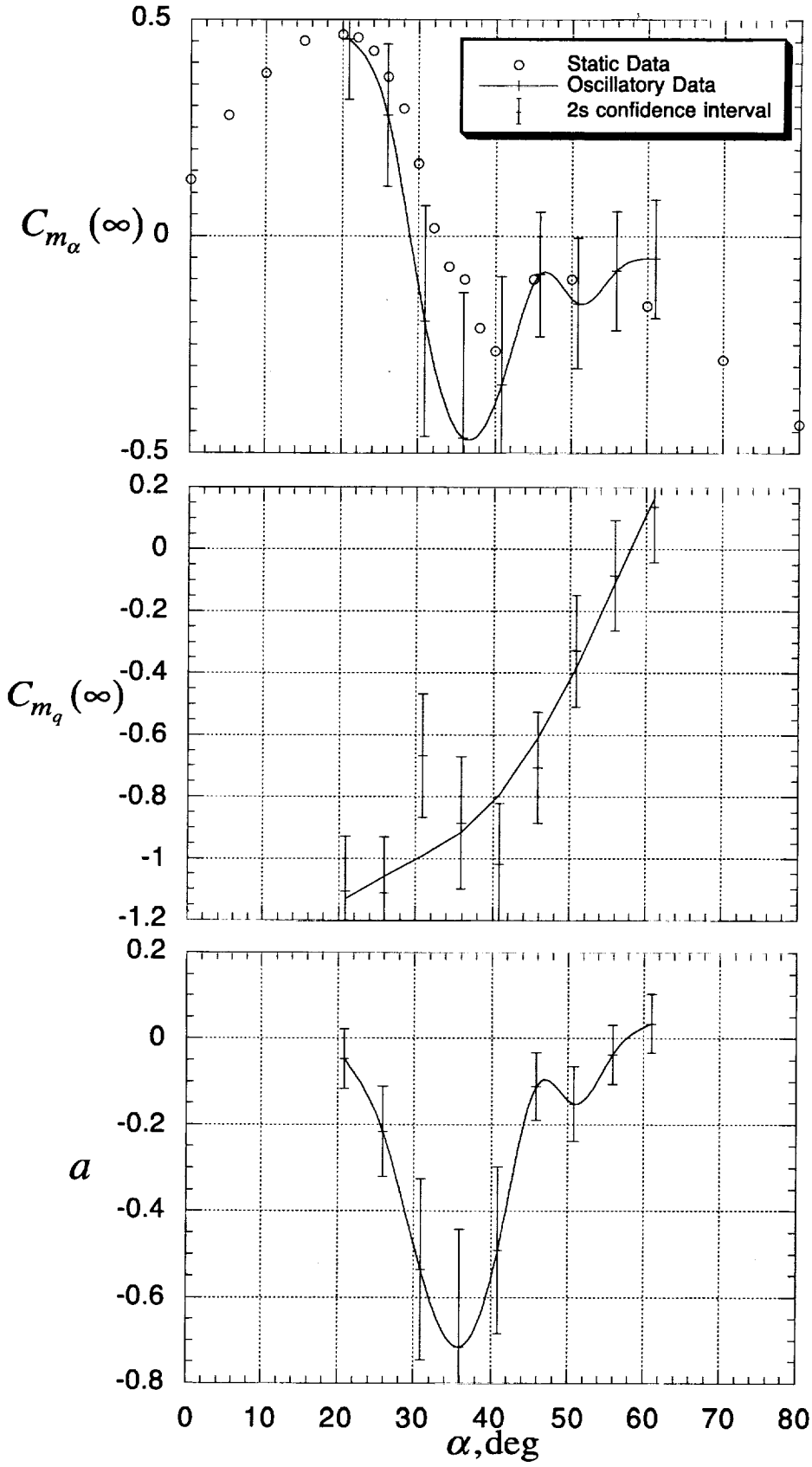

Figure 19. Estimated parameters of pitching-moment components. Model I.

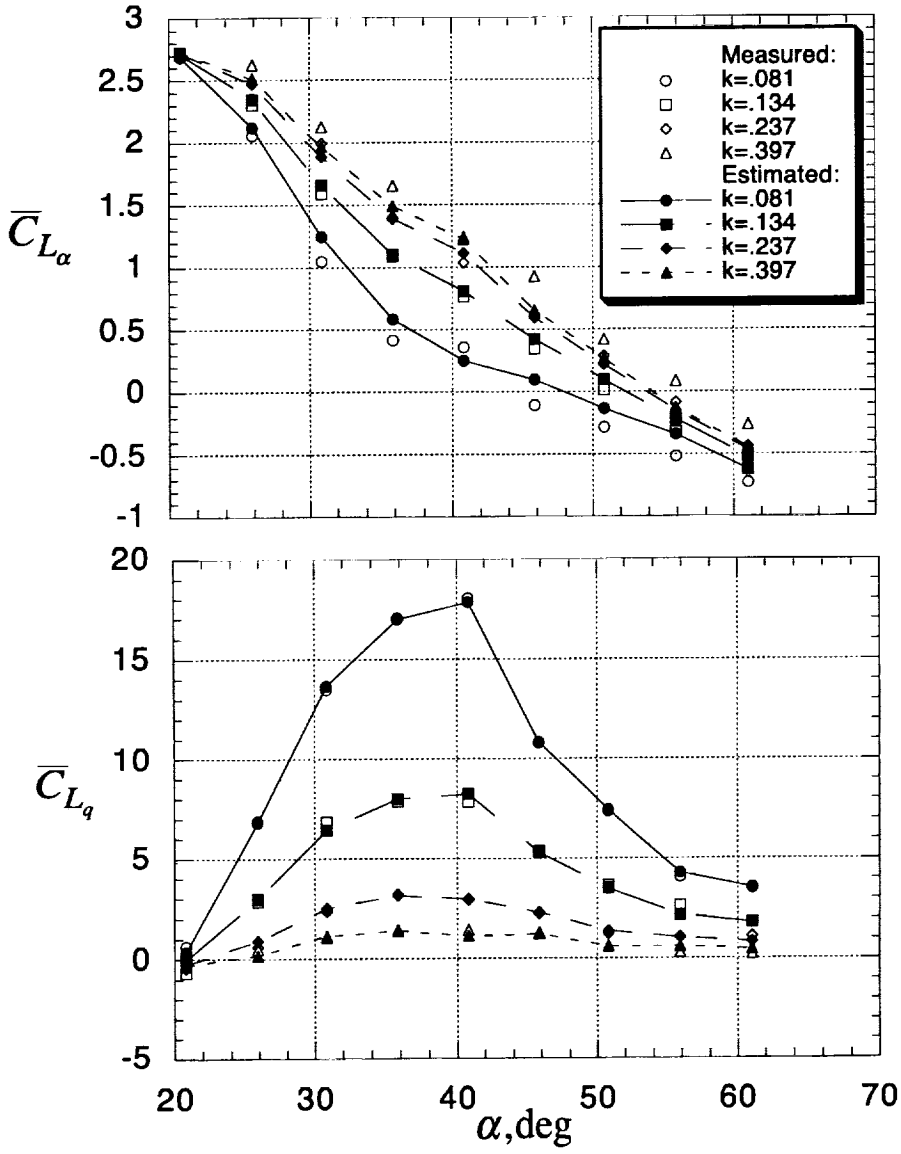

Figure 20. Measured and estimated in-phase and out-of-phase components of lift coefficient. Model I.

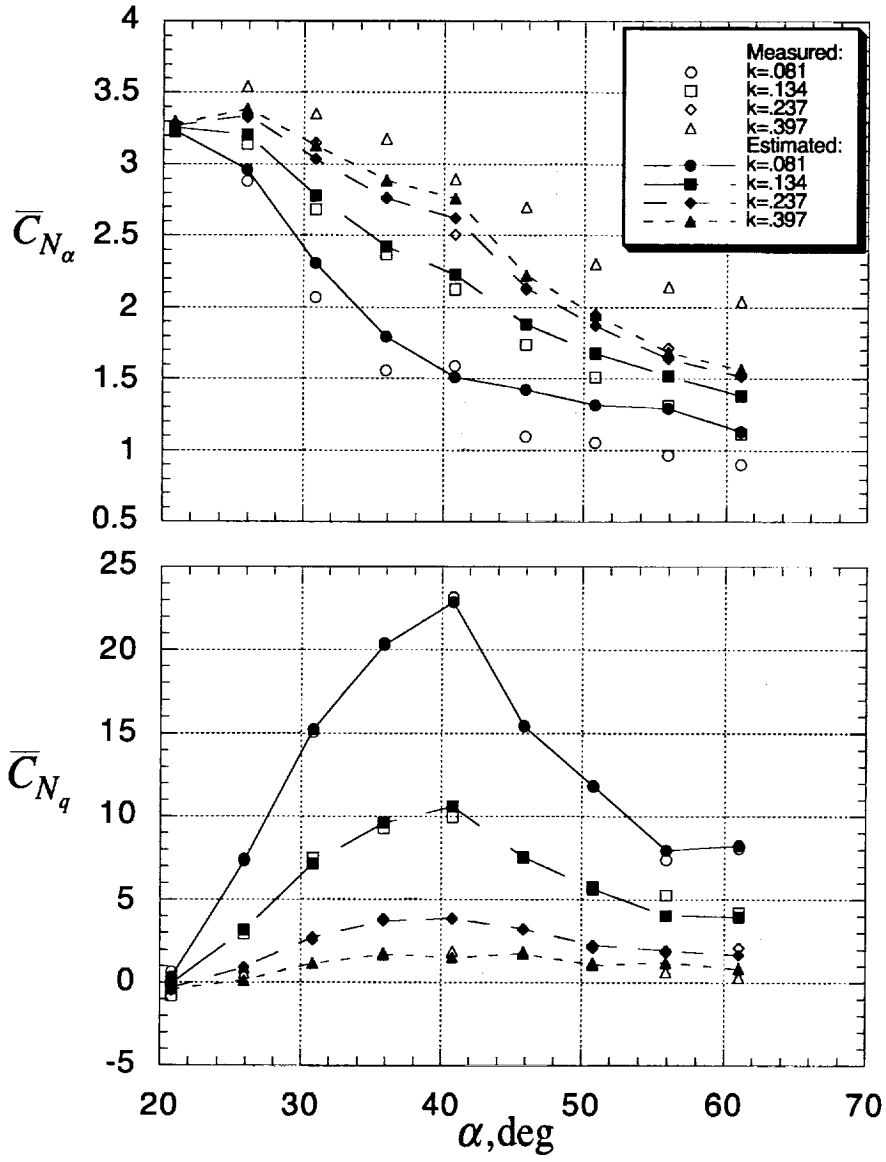

Figure 21. Measured and estimated in-phase and out-of-phase components of normal-force coefficient. Model I.

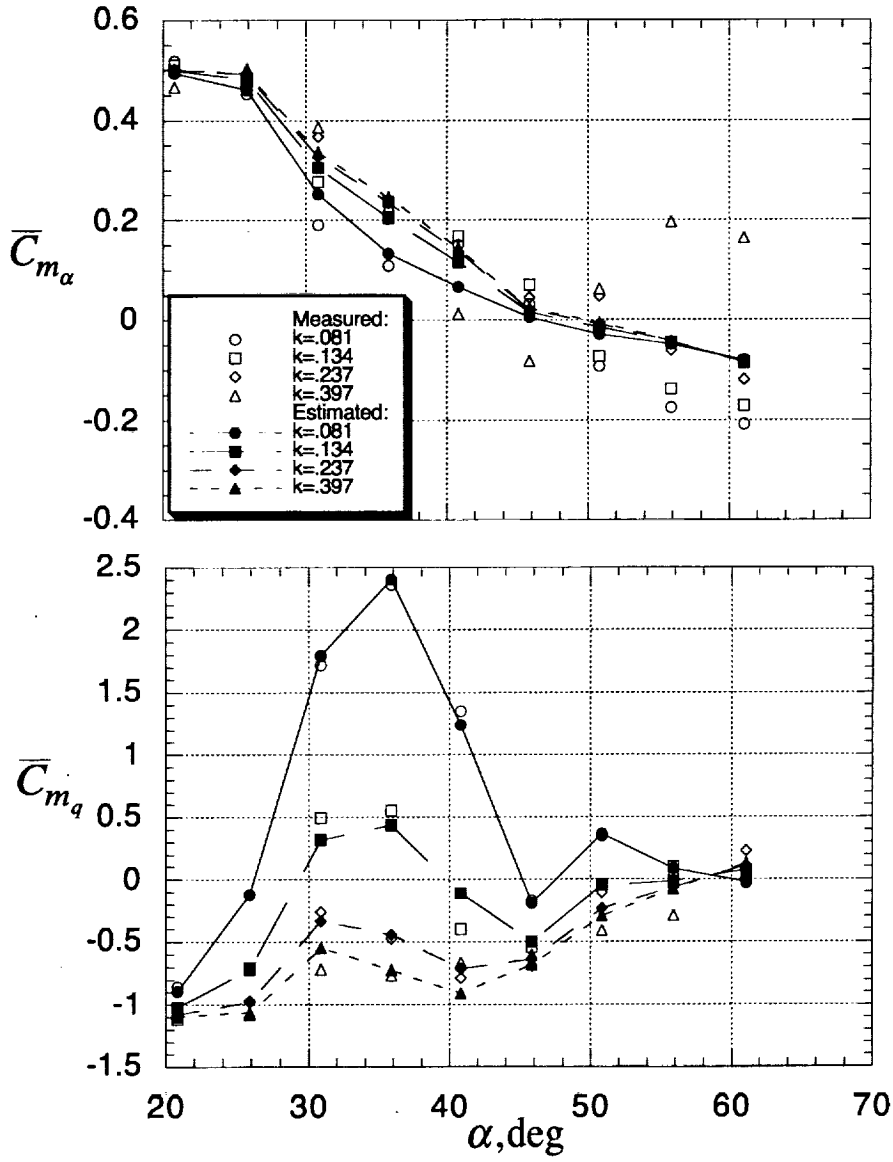

Figure 22. Measured and estimated in-phase and out-of-phase components of pitching-moment coefficient. Model I.

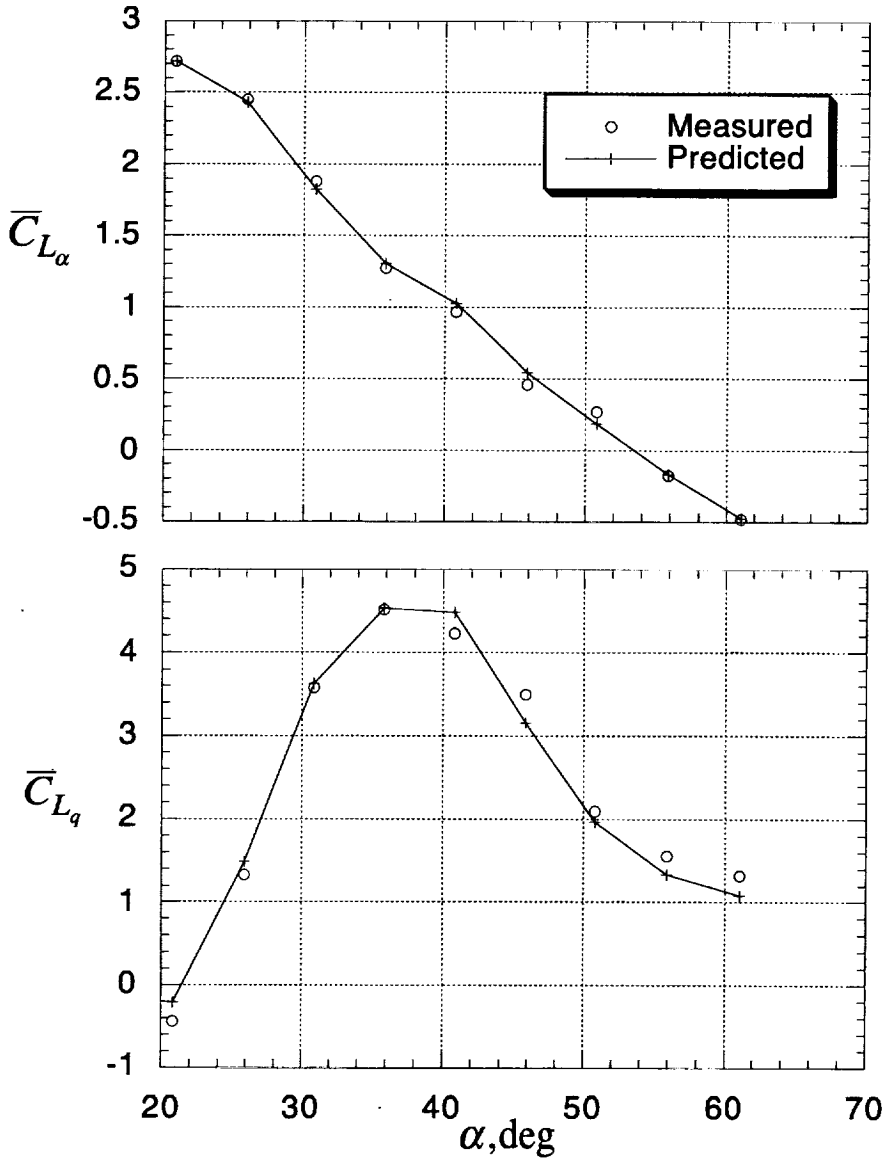

Figure 23. Measured and predicted in-phase and out-of-phase components of lift coefficient. Model I, k=.190.

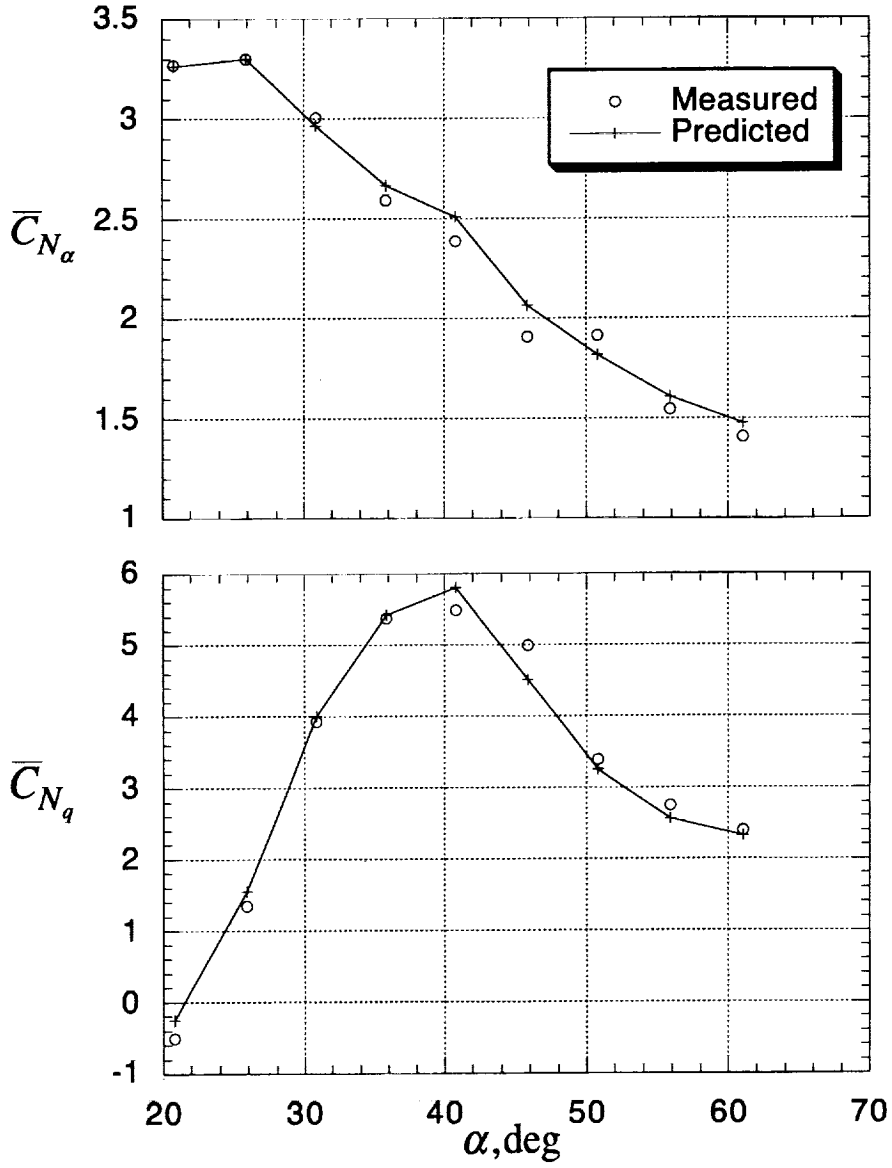

Figure 24. Measured and predicted in-phase and out-of-phase components of normal-force coefficient. Model I, k=.190.

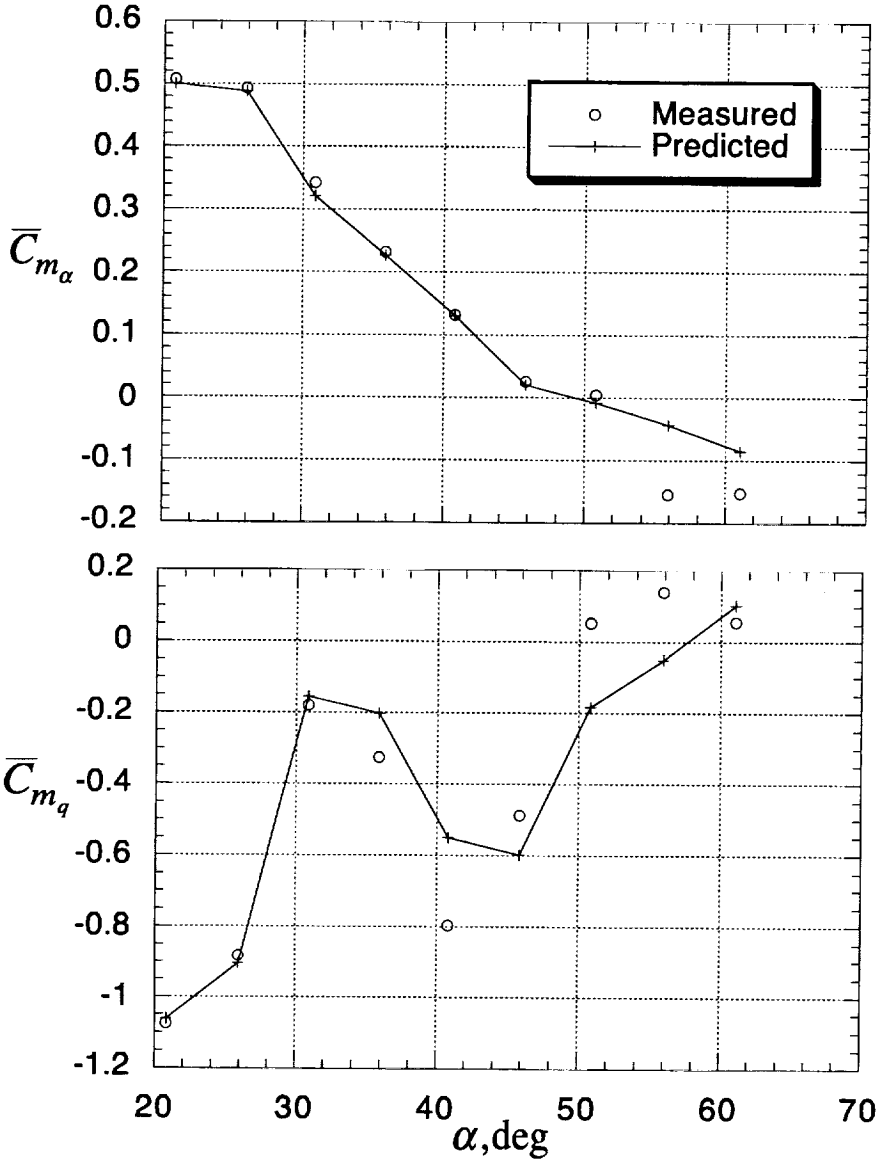

Figure 25. Measured and predicted in-phase and out-of-phase components of pitching-moment coefficient. Model I, k=.190.

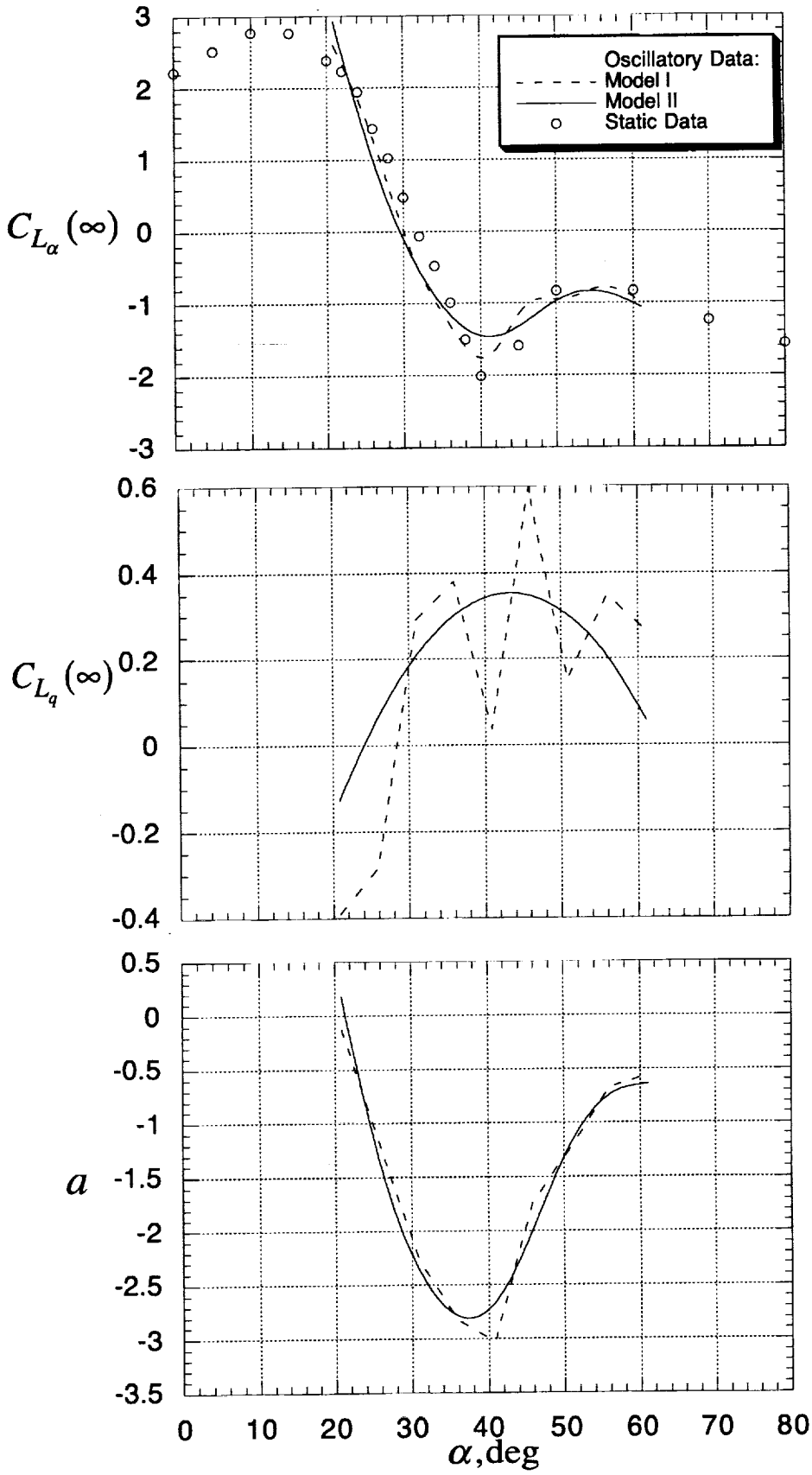

Figure 26. Estimated parameters of lift components.

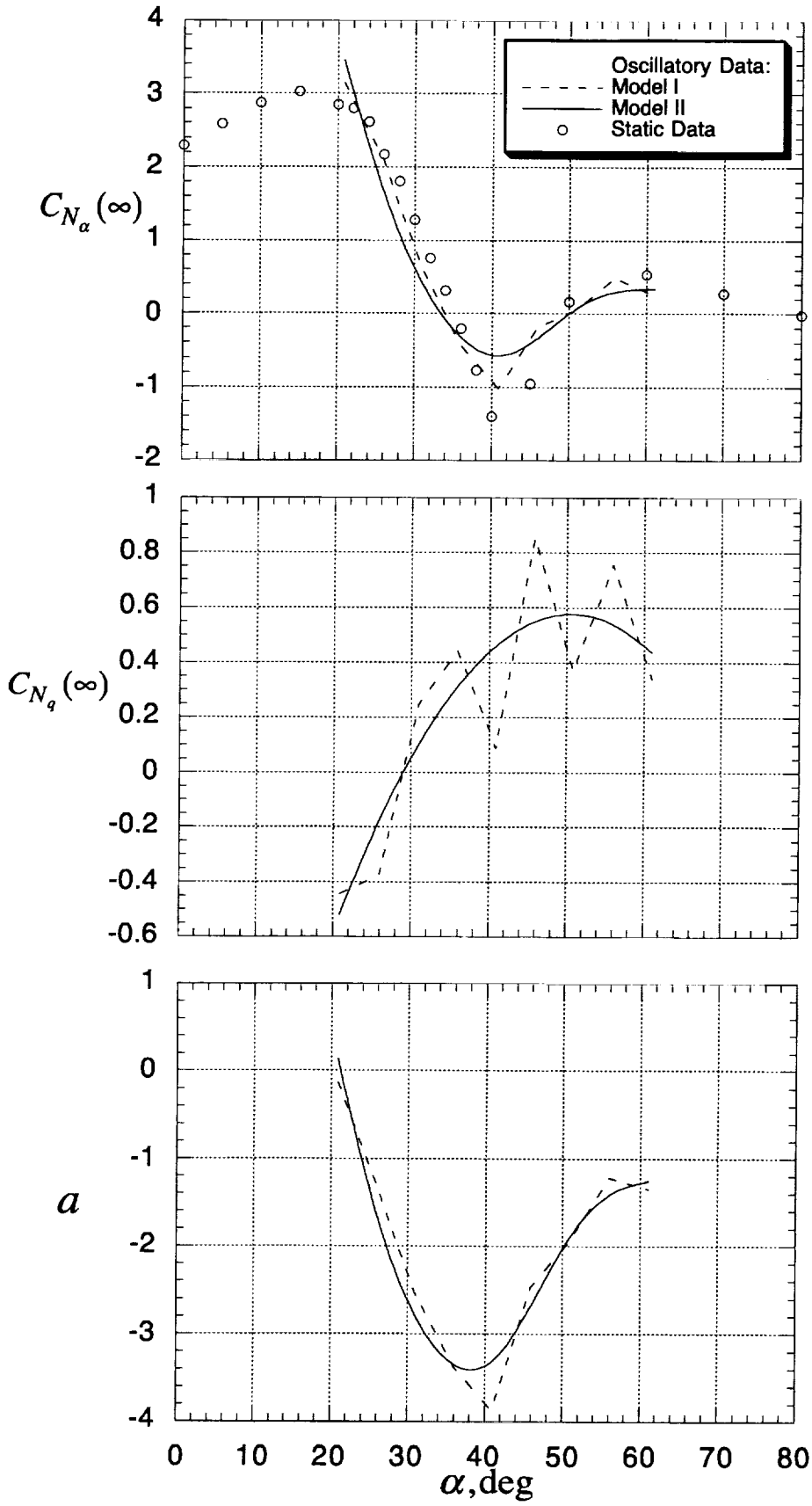

Figure 27. Estimated parameters of normal-force components.

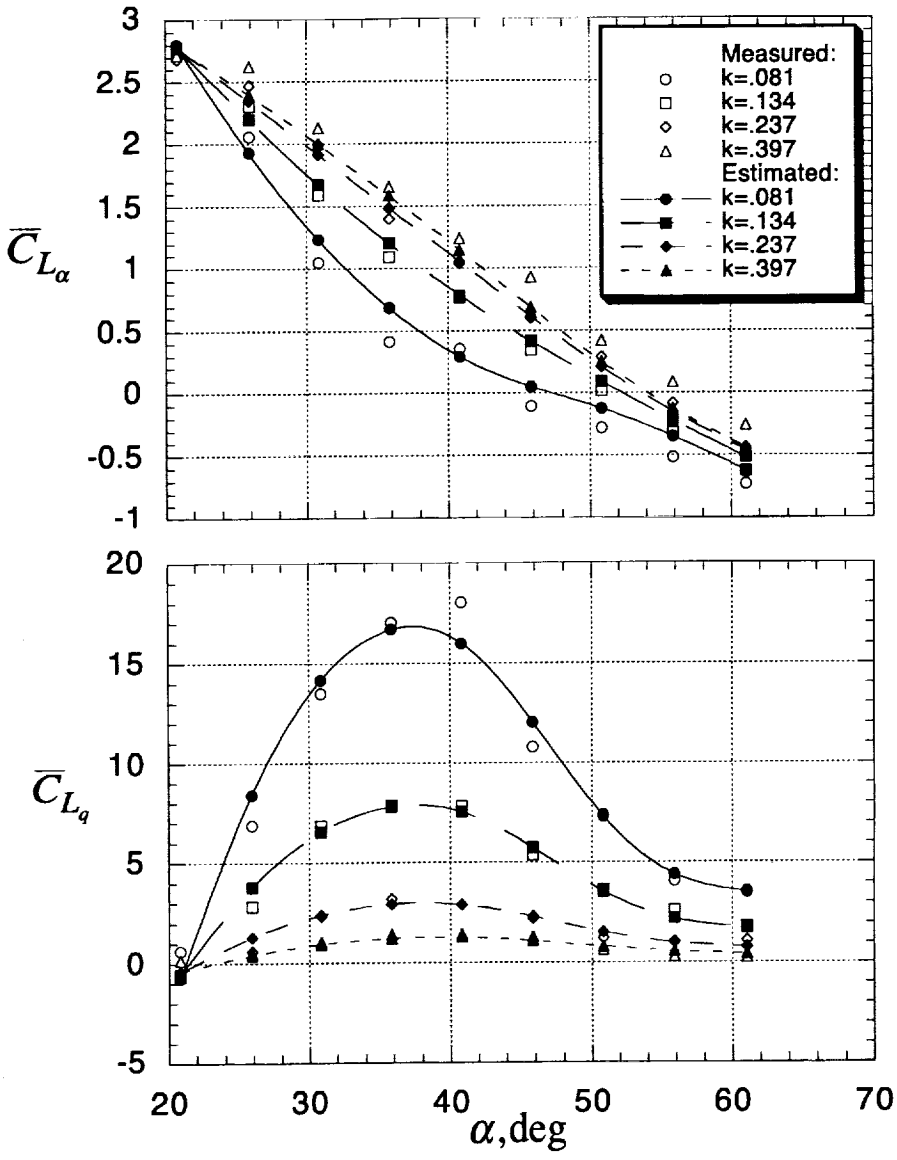

Figure 28. Measured and estimated in-phase and out-of-phase components of lift coefficient. Model II.

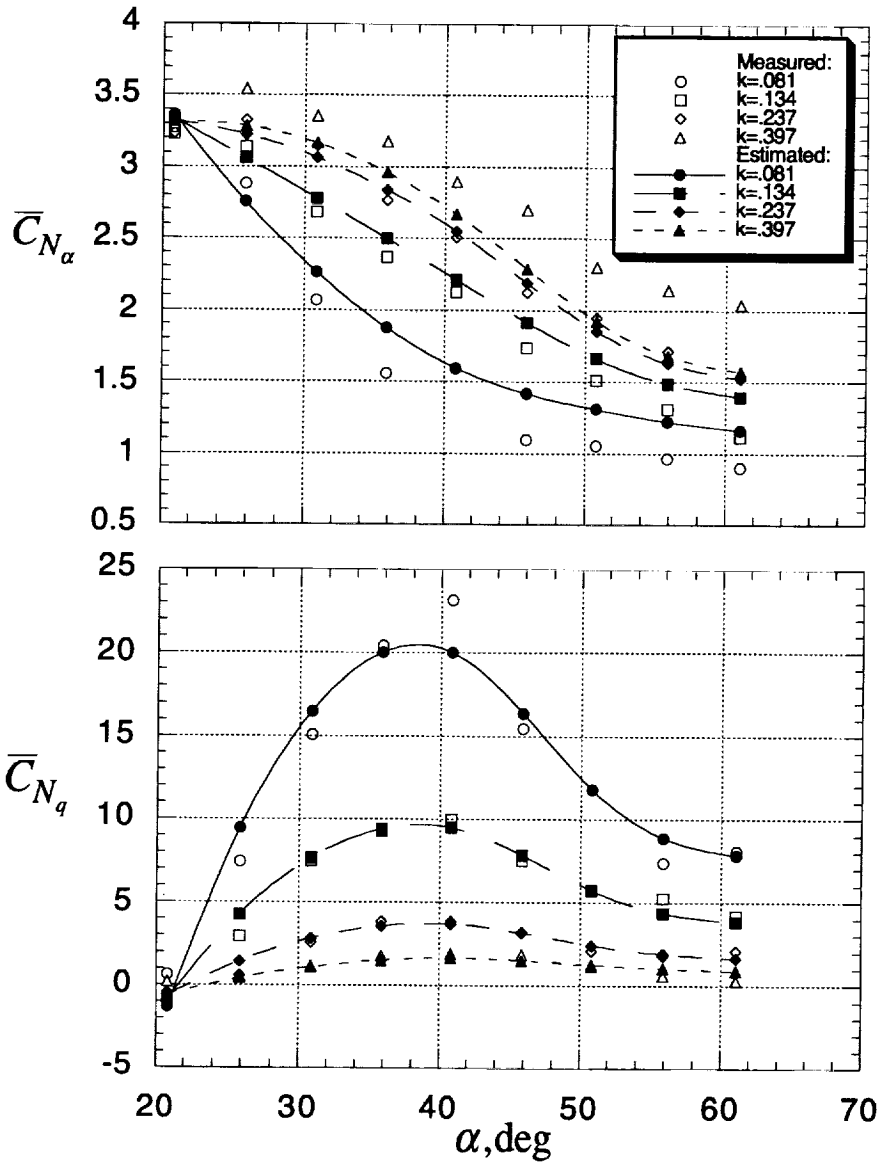

Figure 29. Measured and estimated in-phase and out-of-phase components of normal-force coefficient. Model II.

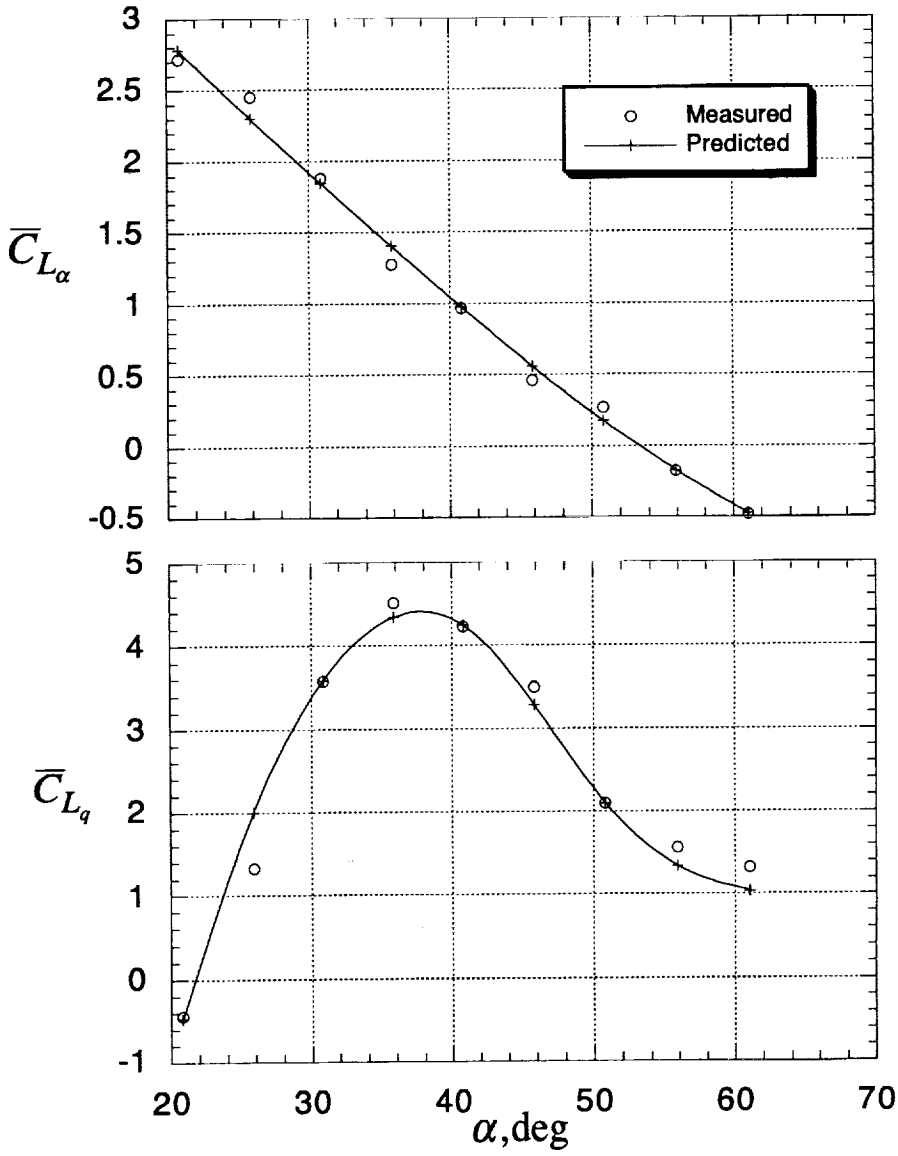

Figure 30. Measured and predicted in-phase and out-of-phase components of lift coefficient. Model II, k=.190.

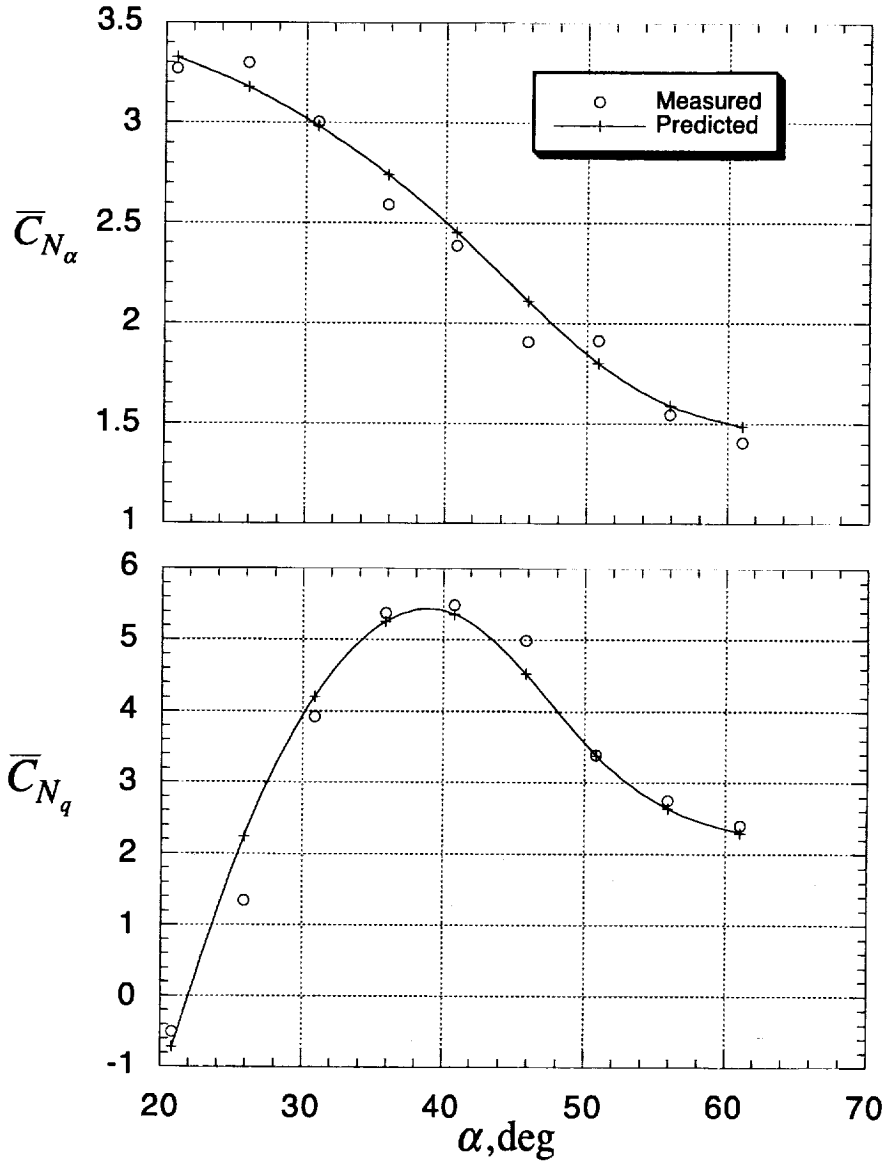

Figure 31. Measured and predicted in-phase and out-of-phase components of normal-force coefficient. Model II, k=.190.

REPORT DOCUMENTATION PAGE

Form Approved
OMB No. 0704-0188

1. AGENCY USE ONLY (*Leave blank*)	2. REPORT DATE	3. REPORT TYPE AND DATES COVERED
	December 1997	Technical Memorandum

4. TITLE AND SUBTITLE
Analysis of Wind Tunnel Longitudinal Static and Oscillatory Data of the F-16XL Aircraft

5. FUNDING NUMBERS
522-33-11-05

6. AUTHOR(S)
Vladislav Klein, Patrick C. Murphy, Timothy J. Curry, and Jay M. Brandon

7. PERFORMING ORGANIZATION NAME(S) AND ADDRESS(ES)
NASA Langley Research Center
Hampton, VA 23681-2199

8. PERFORMING ORGANIZATION REPORT NUMBER
L-17682

9. SPONSORING/MONITORING AGENCY NAME(S) AND ADDRESS(ES)
National Aeronautics and Space Administration
Washington, DC 20546-0001

10. SPONSORING/MONITORING AGENCY REPORT NUMBER
NASA/TM-97-206276

11. SUPPLEMENTARY NOTES
Klein and Curry: George Washington University, Hampton, Virginia
Murphy and Brandon: NASA Langley Research Center, Hampton, Virginia

12a. DISTRIBUTION/AVAILABILITY STATEMENT
Unclassified-Unlimited
Subject Category 08 Distribution: Standard
Availability: NASA CASI (301) 621-0390

12b. DISTRIBUTION CODE

13. ABSTRACT (*Maximum 200 words*)
Static and oscillatory wind tunnel data are presented for a 10-percent-scale model of an F-16XL aircraft. Static data include the effect of angle of attack, sideslip angle, and control surface deflections on aerodynamic coefficients. Dynamic data from small-amplitude oscillatory tests are presented at nominal values of angle of attack between 20 and 60 degrees. Model oscillations were performed at five frequencies from 0.6 to 2.9 Hz and one amplitude of 5 degrees. A simple harmonic analysis of the oscillatory data provided Fourier coefficients associated with the in-phase and out-of-phase components of the aerodynamic coefficients. A strong dependence of the oscillatory data on frequency led to the development of models with unsteady terms in the form of indicial functions. Two models expressing the variation of the in-phase and out-of-phase components with angle of attack and frequency were proposed and their parameters estimated from measured data.

14. SUBJECT TERMS
Wind Tunnel Testing, Static and Oscillatory data, Unsteady Aerodynamics, and Indicial Functions

15. NUMBER OF PAGES
68

16. PRICE CODE
A04

17. SECURITY CLASSIFICATION OF REPORT	18. SECURITY CLASSIFICATION OF THIS PAGE	19. SECURITY CLASSIFICATION OF ABSTRACT	20. LIMITATION OF ABSTRACT
Unclassified	Unclassified	Unclassified	